Charged-particle oscillation in DC voltage biased plane-parallel conductors

Sung Nae Cho*
Micro Devices Group, Micro Systems Laboratory, Samsung Advanced Institute of Technology, Samsung Electronics Co., Ltd, Mt. 14-1 Nongseo-dong, Giheung-gu, Yongin-si, Gyeonggi-do 446-712, Republic of Korea.
(Dated: 16 March 2012)

The phenomenon of charged-particle oscillation in DC voltage biased plane-parallel conductors is discussed. Traditionally accepted mechanism for explaining the oscillatory behavior of charged particles in such system attributes the phenomenon to a process of charge exchange, which takes place when charged-particle is in close proximity to one of the electrodes. A novel finding here reveals that for microscopic or smaller particles under special circumstances, charged-particle oscillation does not involve charge exchanges. Such system radiates and the frequency of emitted radiation is controlled by a DC voltage biased across the two plane-parallel electrodes.

This work has been published in Physics of Plasmas with open access (author select) option. The reference to the article is Phys. Plasmas 19, 033506 (2012); http://dx.doi.org/10.1063/1.3690104.

I. INTRODUCTION

The phenomenon of charged-particle oscillation in DC voltage biased plane-parallel conductors (or electrodes) is well known.[1–3] Such phenomenon has been extensively studied over years, both theoretically and experimentally, due to its usefulness in variety of applications such as electrostatic thruster and nanoprinting, for instance, which require highly energetic charged-nanoparticles with very high speed.[4–8]

Traditionally, the phenomenon of charged-particle oscillation subjected to a constant electric field has been attributed to a process of charge exchange, which takes place when charged-particle is in close proximity to one of the electrodes.[9] When charged-particle is placed between a DC voltage biased plane-parallel electrodes, it migrates to the electrode of opposite polarity. For electrically conducting particles, charge exchange takes place near the point of contact with the electrode. This reverses the polarity of the charged-particle and the particle gets repulsed towards the opposite electrode. There, again, the charge exchange occurs and this process gets repeated, resulting in charged-particle oscillation between the electrodes. Such process is schematically illustrated in Fig. 1.

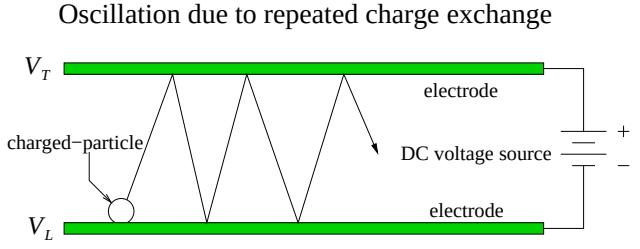

Figure 1: (Color online) Schematic of charged-particle oscillation due to repeated charge exchange.

A novel finding in this work reveals that under special circumstances, core-shell structured charged-particle oscillates under constant electric field. Such oscillatory behavior cannot be explained by the aforementioned traditional picture because it does not involve any charge exchanges. The criterion for such oscillatory modes is given by

$$Q_T > \frac{2\pi\varepsilon_0\kappa_3}{\xi}\left(|\psi|E_p + \sqrt{\psi^2E_p^2 + \frac{16mg\xi}{\pi\varepsilon_0\kappa_3}}\right), \qquad (1)$$

where

$$\xi = \frac{1}{z_{d,m}^2} - \frac{1}{\left(h - z_{d,m}\right)^2} > 0,$$

$$\psi = \frac{\gamma\left(b^3 - a^3\right) - b^3}{z_{d,m}^3} + \frac{\gamma\left(b^3 - a^3\right) - b^3}{\left(h - z_{d,m}\right)^3} - 8 < 0,$$

and

$$\gamma = \frac{3\kappa_3 b^3}{\left(\kappa_2 + 2\kappa_3\right)b^3 + 2\left(\kappa_2 - \kappa_3\right)a^3} < 1.$$

Here, ε_0 is the permittivity of free space, $g = 9.8\,\mathrm{m}\cdot\mathrm{s}^{-2}$ is the gravitational constant, h is the gap between the two plane-parallel electrodes, Q_T is the positive effective charge carried by the core-shell structured particle, m is the mass of the particle, and κ_3 is the dielectric constant for the space between the two electrodes. The core-shell structured particle, which is illustrated in Fig. 2, has a outer radius of b, the inner conductor core radius of a, and the insulator shell layer has a dielectric constant of κ_2. The term $z_{d,m}$ is the maximum value assumed by the parameter z_d in Fig. 2 as the particle executes an oscillatory motion. The particle oscillates back and forth between $z_d = 0$ and $z_d = z_{d,m}$; hence, physically, $z_{d,m}$ represents the turning point where the core-shell structured charged-particle begins to move back towards the conductor plate located at $z_d = 0$.

For a negatively charged core-shell structured particle, the oscillatory criterion is given by

$$|Q_T| > \frac{2\pi\varepsilon_0\kappa_3}{\eta}\left(|\psi|E_p - \sqrt{\psi^2E_p^2 - \frac{16mg\eta}{\pi\varepsilon_0\kappa_3}}\right), \qquad (2)$$

where

$$\eta = \frac{1}{\left(h - z_{d,m}\right)^2} - \frac{1}{z_{d,m}^2} > 0.$$

The two criteria, Eqs. (1) and (2), are not form wise identical due to the fact that negatively charged particle oscillates near the lower conductor plate whereas the positively charged particle oscillates near the upper conductor plate. Here, the upper conductor plate, which is located at $z_d = 0$, is assumed to be held at a higher voltage than the lower conductor plate, which is located at $z_d = h$. The finding in this work reveals that for the configuration illustrated in Fig. 2, the positively charged core-shell structured particle only oscillates in the region where $0 < z_d < h/2$; and, the negatively charged core-shell structured particle oscillates only in the region where $h/2 < z_d < h$.

This remarkable result, which I find it quite obvious but not trivial, is a direct consequence of solving electrostatic boundary value problem involving core-shell structured charged-particle subjected to DC voltage biased plane-parallel electrodes depicted in Fig. 2. The problem is analyzed by first solving the electric potential V_3 in the region M_3. The solution to V_3 is obtained by solving Laplace equation with appropriate electrostatic boundary conditions. Thereafter, induced charges on the surface of each plane-parallel electrodes are computed. Similarly, the effective charge carried by the core-shell structured particle is also computed. The dynamics of the charged-particle is formulated by considering Coulomb forces between the charged-particle and the induced charges on the surface of each plane-parallel electrodes. To generalize the problem to include all particle speed ranges, the dynamics is formulated in relativistic formalism.

This article is organized as follow: (I) introduction, (II) outline of results, (III) theory, (IV) concluding remarks, and (V) acknowledgments. Normally, the section of theory immediately follows the introduction. However, as this work involves lengthy derivations, albeit straightforward, the reader is prone to lose the essence of what this paper tries to portray. For this reason, the section titled "outline of results" is placed immediately after the introduction. In the outline of results, no details of derivations are provided. Instead, the essence of this article is briefly summarized there using only the results, which are rigorously derived in the theory section.

II. OUTLINE OF RESULTS

The essence of this article is to investigate the dynamics of charged-particle illustrated in Fig. 2(a), where a conducting sphere coated with a shell of dielectric is placed in an otherwise constant electric field. The upper conductor plate electrode is held at a DC voltage of V_T and the lower conductor plate electrode is held at DC voltage of V_L, where $V_L < V_T$. The two plane-parallel conductor plate electrodes are separated by a gap of h. The conducting sphere coated with a shell of dielectric has a free charge densities of σ_1 and σ_2, where σ_1 is the free charge density on the surface of the conducting

(a) Particle between parallel conducting plate

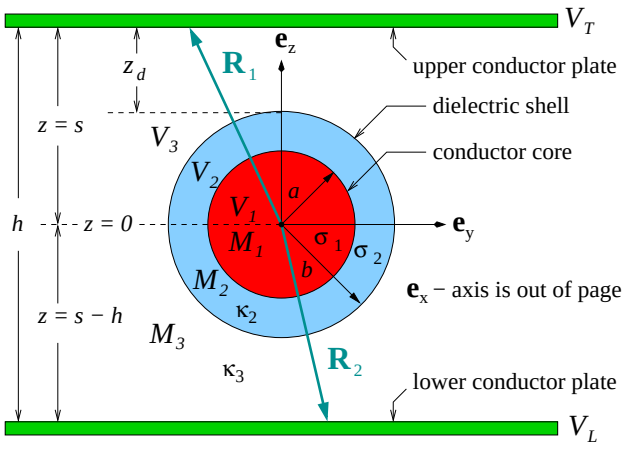

(b) Spherical polar coordinates

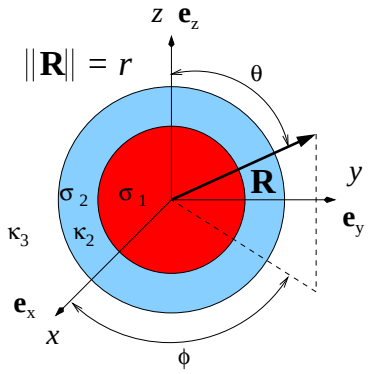

Figure 2: (Color online) (a) Cross-sectional view of an ionized core-shell structured particle confined by the DC voltage biased plane-parallel conductors. (b) Spherical polar coordinate system showing spherical polar triplet (r, θ, ϕ) of a vector $\mathbf{R}$ in Euclidean three dimensional space, $\mathbb{R}^3$.

sphere and σ_2 is the free charge density on the outermost surface of the dielectric shell. The free charge on the surface of dielectric shell has been introduced purely for generalization of the problem. Without loss of generality, σ_2 can be set to zero in the final form of solution.

That said, adopting the particle coordinate system illustrated in Fig. 2(b), the electric potential in region M_3 of Fig. 2(a) is given by

$$V_3(r,\theta) = V_L + E_p(h - s + r\cos\theta) + \frac{\nu}{r} + \frac{\left[\gamma\left(b^3 - a^3\right) - b^3\right] E_p \cos\theta}{r^2} + C, \quad r > b,$$

where C is a constant, E_p is the magnitude of DC electric field in the gap between two parallel plates in the absence of core-shell structured charged-particle,

$$E_p = \frac{1}{h}\left(|V_T - V_L|\right);$$

and, γ and ν are defined as

$$\gamma = \frac{3\kappa_3 b^3}{(\kappa_2+2\kappa_3)b^3+2(\kappa_2-\kappa_3)a^3}, \tag{3}$$

$$\nu = \frac{2a(b-a)\sigma_1}{\varepsilon_0\kappa_2} + \frac{a^2\sigma_1+b^2\sigma_2}{\varepsilon_0\kappa_3}. \tag{4}$$

Here, ε_0 is the electric permittivity of free space and κ_2 and κ_3 are dielectric constants respectively for regions M_2 and M_3 illustrated in Fig. 2. With $V_3(r,\theta)$ and application of appropriate electric boundary conditions to each conductor plates yields

$$\sigma_{iup} = -\varepsilon_0\kappa_3\left\{\frac{3\left[\gamma\left(b^3-a^3\right)-b^3\right]E_p s^2}{\left(\rho^2+s^2\right)^{5/2}} + \frac{\nu s-\left[\gamma\left(b^3-a^3\right)-b^3\right]E_p}{\left(\rho^2+s^2\right)^{3/2}} - E_p\right\}$$

and

$$\sigma_{ilp} = \varepsilon_0\kappa_3\left\{\frac{3\left[\gamma\left(b^3-a^3\right)-b^3\right]E_p(h-s)^2}{\left[\rho^2+(h-s)^2\right]^{5/2}} - \frac{\nu(h-s)+\left[\gamma\left(b^3-a^3\right)-b^3\right]E_p}{\left[\rho^2+(h-s)^2\right]^{3/2}} - E_p\right\},$$

where $\sigma_{iup}\equiv\sigma_{iup}(\rho,s)$ is the induced surface charge density on the surface of upper conductor plate, $\sigma_{ilp}\equiv\sigma_{ilp}(\rho,s)$ is the induced surface charge density on the surface of lower conductor plate, and $\rho\equiv\sqrt{x^2+y^2}$.

The net force exerted on the core-shell structured charged-particle by induced charges on each surfaces of the conductor plates is given by $\mathbf{F}=\mathbf{F}_1+\mathbf{F}_2$,

$$\mathbf{F}_i = -\frac{Q_T}{8\pi\varepsilon_3}\int_{\phi_i=0}^{2\pi}\int_{\rho_i=0}^{\rho}\frac{\varsigma_i\mathbf{R}_i\rho_i d\rho_i d\phi_i}{\left(\mathbf{R}_i\cdot\mathbf{R}_i\right)^{3/2}}, \tag{5}$$

where $i=(1,2)$, $\varsigma_1\equiv\sigma_{iup}$, $\varsigma_2\equiv\sigma_{ilp}$, ε_3 is the electric permittivity of the region M_3, and $\mathbf{R}_i$ is given by

$$\mathbf{R}_1 = \mathbf{e}_x\rho_1\cos\phi_1+\mathbf{e}_y\rho_1\sin\phi_1+\mathbf{e}_z s,$$
$$\mathbf{R}_2 = \mathbf{e}_x\rho_2\cos\phi_2+\mathbf{e}_y\rho_2\sin\phi_2+\mathbf{e}_z(s-h).$$

In the limit the charged-particle becomes very small compared to the dimensions of parallel plates, which is the case for micro- or nano-sized charged-particle confined in a microscopically large, but macroscopically small parallel plates, the $\mathbf{F}_i$ of Eq. (5) for $i=(1,2)$ can be shown to become

$$\mathbf{F}_1 = \mathbf{e}_z\frac{Q_T}{4}\left\{\frac{\nu}{4s^2}+\frac{\left[\gamma\left(b^3-a^3\right)-b^3\right]E_p}{4s^3}-E_p\right\} \tag{6}$$

and

$$\mathbf{F}_2 = \mathbf{e}_z\frac{Q_T}{4}\left\{\frac{\left[\gamma\left(b^3-a^3\right)-b^3\right]E_p}{4(h-s)^3}-\frac{\nu}{4(h-s)^2}-E_p\right\}, \tag{7}$$

where

$$Q_T = 8\pi a(b-a)\sigma_1\frac{\kappa_3}{\kappa_2}+4\pi\left(a^2\sigma_1+b^2\sigma_2\right).$$

When the gravitational effect is included, the force experienced by the core-shell structured charged-particle is

$$\mathbf{F}_T = \mathbf{F}_1+\mathbf{F}_2-\mathbf{e}_z mg$$

or

$$\mathbf{F}_T = \mathbf{e}_z\frac{Q_T}{16}\left\{\frac{\nu}{s^2}-\frac{\nu}{(h-s)^2}+\frac{\left[\gamma\left(b^3-a^3\right)-b^3\right]E_p}{s^3} + \frac{\left[\gamma\left(b^3-a^3\right)-b^3\right]E_p}{(h-s)^3}-8E_p\right\}-\mathbf{e}_z mg, \tag{8}$$

where m is the mass of the particle, $g=9.8\,\mathrm{m}\cdot\mathrm{s}^{-2}$ is the gravity constant, and the gravitational force has been assumed to be in the $-\mathbf{e}_z$ direction. It can be shown that Q_T is related to ν by

$$Q_T = 4\pi\varepsilon_0\kappa_3\nu;$$

and the force $\mathbf{F}_T$ may be re-expressed, for convenience, as

$$\mathbf{F}_T = \mathbf{e}_z\frac{\pi\varepsilon_0\kappa_3\nu}{4}\left\{\frac{\nu}{s^2}-\frac{\nu}{(h-s)^2}+\frac{\left[\gamma\left(b^3-a^3\right)-b^3\right]E_p}{s^3} + \frac{\left[\gamma\left(b^3-a^3\right)-b^3\right]E_p}{(h-s)^3}-8E_p\right\}-\mathbf{e}_z mg. \tag{9}$$

It is noticed that $\mathbf{F}_T$, which is the net force exerted on the core-shell structured charged-particle illustrated in Fig. 2(a), is a one dimensional force that only depends on the relative length, s, measured between the particle and the surface of the upper parallel plate electrode.

The dynamics of oscillating charged-particle is given by

$$\mathbf{e}_z\frac{d}{dt}\left(\frac{m\nu}{\sqrt{1-\frac{\nu^2}{c^2}}}\right) = \mathbf{F}_T,$$

where $c=3\times10^8\,\mathrm{m}\cdot\mathrm{s}^{-1}$ is the speed of light in vacuum. Using the explicit expression for $\mathbf{F}_T$, Eq. (9), it can be shown that

$$\ddot{s} = \left(1-\frac{\dot{s}^2}{c^2}\right)^{3/2}\left(\frac{\pi\varepsilon_0\kappa_3\nu}{4m}\left\{\frac{\nu}{s^2}-\frac{\nu}{(h-s)^2} + \frac{\left[\gamma\left(b^3-a^3\right)-b^3\right]E_p}{s^3} + \frac{\left[\gamma\left(b^3-a^3\right)-b^3\right]E_p}{(h-s)^3}-8E_p\right\}-g\right),$$

where $\mathbf{e}_z$ has been dropped for convenience and the notations $\dot{s}$ and $\ddot{s}$ respectively denote the first and second time derivatives, i.e., $\dot{s} \equiv ds/dt$ and $\ddot{s} \equiv d^2s/dt^2$.

In terms of the z_d parameter illustrated in Fig. 2(a),

$$s = z_d + b, \quad \dot{s} = \dot{z}_d, \quad \ddot{s} = \ddot{z}_d,$$

which is the separation length between the upper electrode plate and the uppermost surface of the core-shell structured charged-particle, the previous nonlinear ordinary differential equation becomes

$$\ddot{z}_d = \left(1 - \frac{\dot{z}_d^2}{c^2}\right)^{3/2} \left(\frac{\pi \varepsilon_0 \kappa_3 v}{4m} \left\{ \frac{v}{(z_d + b)^2} - \frac{v}{(h - z_d - b)^2} + \frac{\left[\gamma\left(b^3 - a^3\right) - b^3\right] E_p}{(z_d + b)^3} + \frac{\left[\gamma\left(b^3 - a^3\right) - b^3\right] E_p}{(h - z_d - b)^3} - 8E_p \right\} - g \right). \tag{10}$$

To solve and plot Eq. (10), the core-shell structured particle in Fig. 2 has been chosen to be the aluminum nanoparticle, where the core is aluminum and the shell is aluminum oxide. The following parameter values have been assigned:

$$\begin{cases} \kappa_2 = 6, \quad \kappa_3 = 1, \\ a = 1.5\,\mu\text{m}, \quad h = 1\,\text{mm}, \\ b - a = 4\,\text{nm}, \\ V_T = 8\,\text{kV}, \quad V_L = 0\,\text{V}, \\ \sigma_1 = 0.014\,\text{C}\cdot\text{m}^{-2}, \\ \sigma_2 = 0\,\text{C}\cdot\text{m}^{-2}, \\ \rho_{m,1} = 2700\,\text{kg}\cdot\text{m}^{-3}, \\ \rho_{m,2} = 3800\,\text{kg}\cdot\text{m}^{-3}, \end{cases} \tag{11}$$

where $\rho_{m,1}$ and $\rho_{m,2}$ are mass densities of the aluminum core and the aluminum oxide, respectively. The thickness of aluminum oxide layer has been set at 4 nm, which is typical of aluminum nanoparticles.[10] Because aluminum oxide is an high-k dielectric material, i.e., $k_2 \sim 6$, the σ_2 has been set to zero.[11] For an insulator, the value of σ_2 is negligible compared to σ_1. The mass of the core-shell structured particle has been computed as

$$m = \underbrace{\frac{4}{3}\pi a^3 \rho_{m,1}}_{m_c} + \underbrace{\frac{4}{3}\pi\left(b^3 - a^3\right)\rho_{m,2}}_{m_s}, \tag{12}$$

where m_c and m_s represent the masses of the core and the shell, respectively. With these values assigned for each of the parameters, Eq. (10) is solved via Runge-Kutta method subjected to the following initial conditions,

$$z_d(0) = 0.25h \quad \text{and} \quad \dot{z}_d(0) = 0, \tag{13}$$

which conditions are schematically illustrated in Fig. 3.

In this work, it is assumed that core-shell structured charged-particle is already ionized. And, for the initial conditions, this ionized particle just happens to be at $z_d = 0.25h$ with no initial speed. Then, the question to be asked in this work is this; what happens to the dynamics of this charged particle afterwards? Before I present the result of dynamics, I shall discuss how such particle might be ionized experimentally.

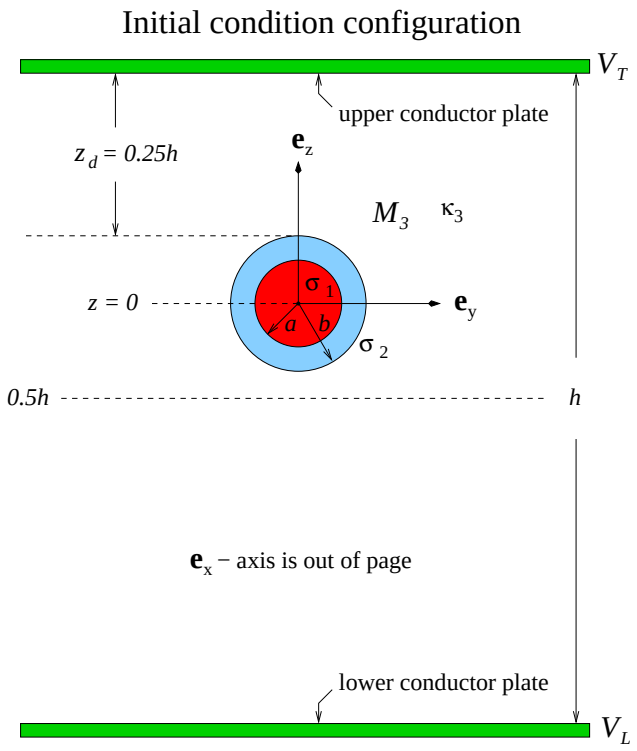

Figure 3: (Color online) Initial position of the particle. There are no free surface charges on the insulating shell; and, hence, $\sigma_2 = 0\,\text{C}\cdot\text{m}^{-2}$.

Szirmai demonstrated that a core-shell structured particle, i.e., an aluminum core surrounded by a thin layer of aluminum oxide, can be charged by exposing it to a static electric field of sufficiently large strength. At the onset of the field emission, electrons are stripped from the particle's conductive core and tunnel through a thin dielectric layer, leaving the particle net positively charged as a whole.[12] Because electrons are more strongly bonded in a dielectric, it takes significantly larger electric field to ionize insulators. Therefore, it is reasonable to assume no free surface charges on the insulating shell in Fig. 3, implying $\sigma_2 = 0\,\text{C}\cdot\text{m}^{-2}$ there.

The field emission process strongly depends on the geometry as well as on the orientation of host material.[13–17] For instance, a spherical surface has a lower field emission threshold point than a flat surface; which is also the reason why a conductive needle emits electron better than a thick rod conductor. Physically, a sharp tip can be described by a surface with large curvature whereas the dull one is described by a surface with smaller curvature. By definition, the curvature of a circle of radius r is large for small r and is small for large r. Accordingly, spherical nanoparticles have very large curvature whereas macroscopic spherical particles have very small curvature. What is referred to as a flat surface is just a spe-

cial case in which the radius r of a sphere becomes infinite in extent. Since the conductive needle emits electrons better than a thick rod conductor, a needle has a lower field emission threshold than a rod. This implies that smaller spherical conductors, such as nanoparticles, have lower field emission threshold than larger spherical conductors or flat surfaces. That explained, the field emission thresholds are schematically summarized in Fig. 4 for a spherical conductor, spherical dielectric, and a conductor plate, wherein the following field emission thresholds are assumed: (a) E_{cs} for the conducting sphere, (b) E_{ds} for the dielectric sphere, and (c) E_{cp} for the conductor plate in vacuum. Since the geometry of conductor plates is just an extension of infinitely large sphere, the finite sized conducting spheres have lower field emission threshold than large conductor plates; and, thus, $E_{cp} > E_{cs}$. Because electrons are very strongly bonded in a dielectric, exceptionally large electric field must be applied to strip an electron from a dielectric material. In general, it is much easier to strip an electron from a conductor plate than from a dielectric. Hence, it is reasonable to assume $E_{ds} > E_{cp}$. In summary, the three field emission thresholds satisfy the inequality given by

$$E_{ds} > E_{cp} > E_{cs} > 0,$$

where E_{ds}, E_{cp}, and E_{cs} are field emission thresholds for dielectric sphere, conductor plate, and conductor sphere, respectively.

What if the conducting spherical particle is coated with a thin layer of a dielectric shell, just like the one illustrated in Fig. 3; would it be still possible to ionize such particle by a process of field emission? The answer to this is yes, of course. For instance, Konopsky et al. have experimentally measured field emissions from sharp silicon tips covered with thin dielectric calcium fluoride layers.[18] Iwasaki and Sudoh investigated electron tunneling through an aluminum oxide thin film on a nickel-aluminum metal composite.[19] And, Kurnosikov et al. have also investigated electron transport through alumina oxide tunnel junctions.[20] Nevertheless, the insulating dielectric shell on the surface of spherical conductor increases the minimum electric field required to ionize a particle. Then, to ionize a core-shell structured particle, it is crucial that two plane-parallel conductor plates are able to produce electric field large enough to ionize a particle without electric discharge setting in. When there is a field emission originating from one of the conductor plates, i.e., the lower conductor plate in Fig. 3, the positively ionized core-shell structured particle quickly neutralizes. To prevent this, the two plane-parallel conductor plates must be able to produce sufficiently large electric field to ionize the particle, but at the same time this electric field must not be large enough to initiate field emission from conductor plates themselves.

Zouache and Lefort investigated the phenomenon of electric discharge in plane-parallel conductor plates, such as the one illustrated in Fig. 3, but without particle inside.[21] In their configuration, two plates are separated by an empty space gap of one micron in length. They have tested various materials for the conductor plates. Among various materials tried for conductor plates, one was prepared from a mixture of 60% silver and 40% nickel in its material composition. Conductor plates with such material composition generated electric discharge at applied electric field strength of $E_p \approx 3850\,\mathrm{MV\cdot m^{-1}}$. In a vacuum gap separated plane-parallel conductor plates, electric discharge is attributed to electrons from lower potential plate tunneling through the gap towards the plate with higher potential, thereby shorting the two plates and causing an electric discharge. In this regard, the phenomenon of electric discharge is intrinsically connected to the field emission threshold illustrated in Fig. 4(c). Hence, in the aforementioned Zouache and Lefort's configuration, the field emission threshold of $E_{cp} \lesssim 3850\,\mathrm{MV\cdot m^{-1}}$ can be roughly approximated. This field emission threshold value may be compared with the electric field used by Szirmai to ionize his particle. In Szirmai's experiment, an electric field of $E_p \approx 4.67\,\mathrm{MV\cdot m^{-1}}$ was sufficient to produce a net charge of $\sim 4\times10^{-15}\,\mathrm{C}$ on a core-shell structured spherical aluminum particle of $3\,\mu\mathrm{m}$ in diameter. For the particle in Szirmai's experiment, the field emission threshold of $E_{cs} \lesssim 4.67\,\mathrm{MV\cdot m^{-1}}$

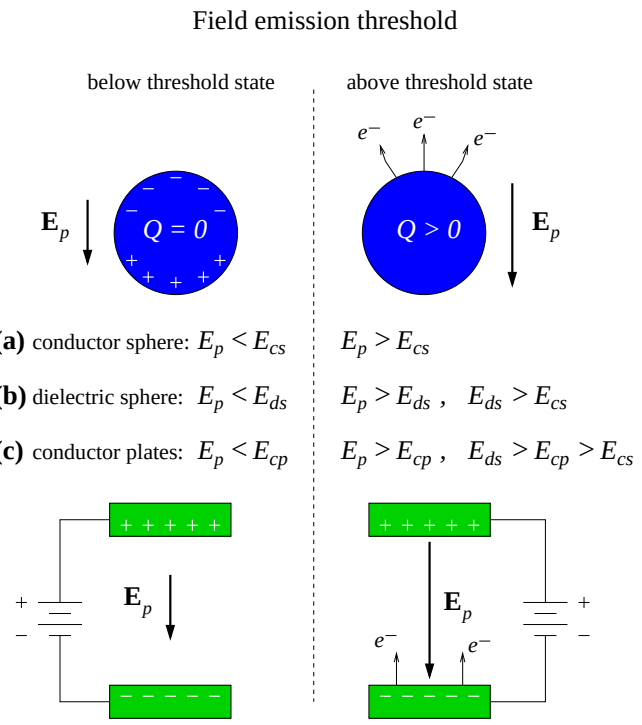

Figure 4: (Color online) Schematic of electron field emission threshold. When the magnitude $E_p \equiv \left\|\mathbf{E}_p\right\|$ of applied electric field is less than the field emission threshold, spherical particle is polarized inside, but no electrons are field emitted and the particle as a whole remains neutral, i.e., $Q = 0$. When E_p exceeds the field emission threshold, electrons are stripped (or field emitted) from the particle, leaving the particle net positively charged, i.e., $Q > 0$. Similarly, when E_p is below the field emission threshold, no electrons are emitted from the lower potential plate. However, when E_p exceeds the field emission threshold, electrons from lower potential plate begin to tunnel across the vacuum gap and electric discharge sets in. In the figure, field emission electrons are indicated by e^-.

can be assumed. Comparing the two values, one finds

$$\frac{E_{cp}}{E_{cs}} = \frac{3850\,\mathrm{MV}\cdot\mathrm{m}^{-1}}{4.67\,\mathrm{MV}\cdot\mathrm{m}^{-1}} \approx 824,$$

which result suggests that for the configuration illustrated in Fig. 3, the particle can be sufficiently ionized when Zouache and Lefort's conductor plates are used. Further, by limiting applied electric field to a value much smaller than E_{cp} and, yet, much larger than E_{cs}, the particle can be ionized in the absence of field emission electrons originating from the plate held at lower potential. This prevents the ionized particle from neutralizing. For instance, the electric field value of $E_p \approx 0.5E_{cp}$ or $E_p \approx 412E_{cs}$ is much smaller than E_{cp}, but it is still much larger than E_{cs}.

Aforementioned process of charging by field emission is schematically summarized in Fig. 5. To illustrate the mechanism, particular electrons in the particle's shell and the core regions are labeled e_1^- and e_2^-, respectively. Similarly, particular electrons in the lower conductor plate are labeled e_3^- and e_4^-. It is understood that particle as a whole is initially electrically neutral, implying $Q = 0$. That cleared, an applied static electric field of magnitude $E_p \equiv \left\|\mathbf{E}_p\right\|$, where

$$E_p \gg E_{cs}, \;\; \text{but} \;\; E_p \ll E_{cp} < E_{ds}, \tag{14}$$

is produced by connecting two plane-parallel conductor plates to a battery. Since $E_p \gg E_{cs}$, where E_{cs} is the field emission threshold for the particle's conductor core (see Fig. 4), e_2^- tunnels through the dielectric shell and the particle as a whole becomes net positively charged. Because $E_p \ll E_{ds}$, where E_{ds} is the field emission threshold for the particle's dielectric shell, no electrons are physically stripped from the shell and e_1^- remains confined to the shell, leaving the shell electrically neutral. Similarly, because $E_p \ll E_{cp}$, where E_{cp} is the field emission threshold for the lower conductor plate, no electrons can escape the surface of the lower conductor plate. The electrons, i.e., e_3^- and e_4^-, may redistribute themselves, but cannot physically escape the conductor plate's surface; which is the reason why e_4^- cannot tunnel through the particle's dielectric shell to neutralize the positively charged core. To do so, e_4^- must first escape the plate's surface, which is not possible since $E_p \ll E_{cp}$. In conclusion, once the particle is charged and the electric field satisfies the condition defined in Eq. (14), the core-shell structured particle remains positively charged.

Figure 5 presents a way to prepare yet another initial configuration, which is different from the one illustrated in Fig. 3, for the differential equation of Eq. (10). I shall briefly outline how such initial configuration might be prepared from Fig. 5. Starting with initially uncharged core-shell structured particle, the particle is ionized following the scheme illustrated in Fig. 5. Once the core-shell structured particle has been sufficiently ionized, the entire system is physically flipped over. Don't worry about the particle falling down because it won't. In fact, the positively charged particle sticks to the surface of the conductor plate held at lower of the two potentials. The reason for this is explained later in this section when the types of forces involved in the system are discussed. With the configuration illustrated in Fig. 5 flipped over, the initial conditions

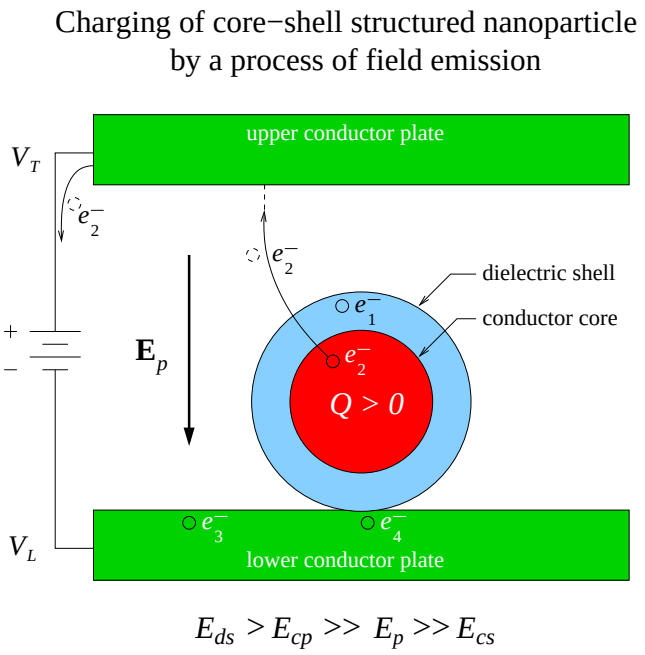

Figure 5: (Color online) Schematic illustration of ionization process of core-shell structured nanoparticle. For the illustration purpose, particular electrons in the particle's shell and the core regions are labeled e_1^- and e_2^-, respectively. Similarly, particular electrons in the lower conductor plate are labeled e_3^- and e_4^-. Initially, the particle as a whole is neutral and $Q = 0$. After the field emission, the particle as a whole becomes net positively charged, $Q > 0$.

are now specified by

$$z_d(0) = 0 \quad \text{and} \quad \dot{z}_d(0) = 0.$$

In the flipped over configuration, the applied electric field $\mathbf{E}_p$ is in the $\mathbf{e}_z$ direction. Now, to make this configuration suitable for the differential equation of Eq. (10), the direction of applied electric field must be reversed. Thus, reversing the direction of $\mathbf{E}_p$ to $-\mathbf{e}_z$ direction, this configuration becomes identical to the initial configuration illustrated in Fig. 3, except now $z_d(0) = 0$ instead of $z_d(0) = 0.25h$. Either choice is good for the initial condition of $z_d(t)$. That said, I shall keep using the initial conditions specified in Eq. (13) and the initial configuration illustrated in Fig. 3 for the rest of this work.

Returning to the plotting of z_d from Eq. (10) with initial conditions specified in Eq. (13), the particle position as function of time has been plotted in Fig. 6 using the parameter values defined in Eq. (11). The upper electrode is located at $z_d = 0\,\mathrm{m}$ in the plot. As it can be observed from the plot, the core-shell structured charged-particle executes an oscillatory motion between the two plane-parallel electrodes; and, such motion does not involve charge exchanges. One knows this because the governing equation of motion, i.e., Eq. (10), has been derived without any assumption of charge exchange. Such oscillatory behavior is fundamentally different from the traditional picture, which process assumes charge exchange mechanisms. The core-shell structured charged-particle rebounds at $z_d \approx 2.5 \times 10^{-4}\,\mathrm{m}$ from the upper conductor plate.

This rebounding position is too far from the lower conductor plate to account for any charge exchange processes even in the physical situations. In the plot of Fig. 6, the lower conductor plate is located at $z_d \approx h = 0.001\,\mathrm{m}$.

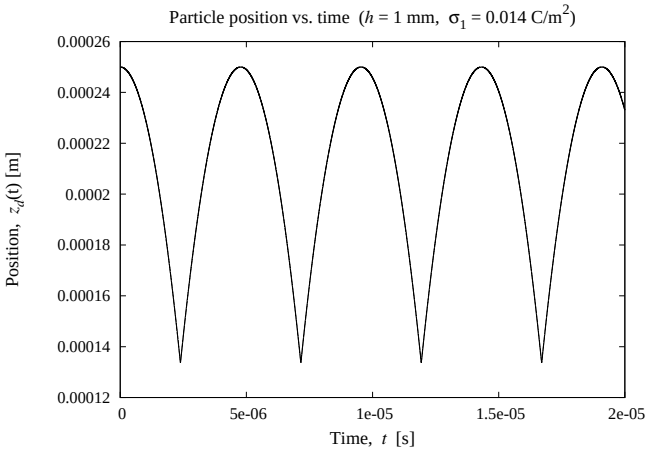

Figure 6: Particle distance from the surface of upper conductor plate as function of time. For the plot, the values defined in Eq. (11) have been used with initial conditions specified in Eq. (13). $V_T - V_L = 8\,\mathrm{kV}$ implies an applied electric field of $E_p = 8\,\mathrm{MV\cdot m^{-1}}$. The upper electrode is located at $z_d = 0\,\mathrm{m}$.

Hereafter, it is understood that charged-particle oscillation does not involve any charge exchanges for the rest of this paper. That said, what's the criterion for charged-particle oscillation? Oscillatory modes occur when the effective charge carried by the positively charged particle satisfies the condition given by

$$Q_T > \frac{2\pi\varepsilon_0\kappa_3}{\xi}\left(|\psi|E_p + \sqrt{\psi^2E_p^2 + \frac{16mg\xi}{\pi\varepsilon_0\kappa_3}}\right),$$

where

$$\xi = \frac{1}{z_{d,m}^2} - \frac{1}{\left(h - z_{d,m}\right)^2} > 0,$$

$$\psi = \frac{\gamma\left(b^3 - a^3\right) - b^3}{z_{d,m}^3} + \frac{\gamma\left(b^3 - a^3\right) - b^3}{\left(h - z_{d,m}\right)^3} - 8 < 0,$$

and

$$\gamma = \frac{3\kappa_3 b^3}{\left(\kappa_2 + 2\kappa_3\right)b^3 + 2\left(\kappa_2 - \kappa_3\right)a^3} < 1.$$

Similarly, for a negatively charged core-shell structured particle, the oscillatory criterion is given by

$$|Q_T| > \frac{2\pi\varepsilon_0\kappa_3}{\eta}\left(|\psi|E_p - \sqrt{\psi^2E_p^2 - \frac{16mg\eta}{\pi\varepsilon_0\kappa_3}}\right),$$

where

$$\eta = \frac{1}{\left(h - z_{d,m}\right)^2} - \frac{1}{z_{d,m}^2} > 0.$$

The mass dependence in Eqs. (1) and (2) reveals that particle with larger mass requires significantly larger effective charge compared to the particle with smaller mass to initiate oscillatory motion. Initially neutral particle can be charged or ionized by exposing it to a strong static electric field. For a nanoparticle, large portion of atoms composing it participate in the ionization, yielding in relatively large charge density per mass. However, for a macroscopic particle or an object, a great portion of atoms composing it does not participate in the ionization process and only those near the surface participate in the ionization due to electric field shielding effects. As a result, macroscopic particles have relatively small charge density per mass. One may argue that the strength of electric field can always be increased to completely ionize the macroscopic particle. That, however, is not possible because, even in vacuum, electric breakdown sets in at some point and everything neutralizes.[21]

Based on this argument, the oscillation criterion specified in Eq. (1) is more likely to be satisfied by microscopic or smaller particles than by macroscopic counterparts. This implies the charged-particle oscillation presented in this paper is more likely to be observed from nanoparticle systems than from systems involving macroscopic particles. I shall now discuss why microscopic particles are more likely to satisfy the criterion of Eqs. (1) or (2) than the macroscopic counterparts. To demonstrate this, I shall consider an aluminum ball of radius $b = 1.5\,\mu\mathrm{m}$ representing the smaller particle and another one with radius $b = 3\,\mathrm{mm}$ representing the larger counterpart. To keep matters simple, I shall assume that the space between electrodes is a vacuum.

In vacuum, $\kappa_3 = 1$ and $\pi\varepsilon_0\kappa_3 = 2.78\times10^{-11}\,\mathrm{N^{-1}\cdot m^{-2}\cdot C^2}$, and the gravity constant is $g = 9.8\,\mathrm{m\cdot s^{-2}}$. The mass densities of aluminum and aluminum oxide are $\rho_{m,1} = 2700\,\mathrm{kg\cdot m^{-3}}$ and $\rho_{m,2} = 3800\,\mathrm{kg\cdot m^{-3}}$, respectively. Thus, for a core radius of $a = 1.5\,\mu\mathrm{m}$ and shell thickness of $b - a = 4\,\mathrm{nm}$, the total mass of the particle is obtained using Eq. (12) to yield $m \approx 3.86\times10^{-14}\mathrm{kg}$. The dielectric constant for the particle's shell is $\kappa_2 = 6$. For the value of $z_{d,m}$, I shall choose $z_{d,m} = 0.25h$, where $h = 1\,\mathrm{mm}$. For the applied electric field, I shall choose $E_p = 8\,\mathrm{kV\cdot m^{-1}}$. Insertion of these values into Eq. (1) yields

$$Q_{T,mic} \equiv Q_T > 5\times10^{-13}\,\mathrm{C}, \tag{15}$$

where the notation $Q_{T,mic}$ denotes the microscopic particle.

Now, I shall compute the same for the macroscopic counterpart. An aluminum ball of core radius $a = 3\,\mathrm{mm}$ and shell thickness of $b - a = 4\,\mathrm{nm}$ has a mass of $m \approx 3.05\times10^{-4}\mathrm{kg}$, where Eq. (12) has been used to compute the mass. To make sure this aluminum ball has sufficient room between the electrodes for oscillation, the gap between the two electrodes is increased to a value of $h = 1\,\mathrm{m}$. Keeping all other values same as previous, Eq. (1) gives

$$Q_{T,mac} \equiv Q_T > 9\times10^{-7}\,\mathrm{C}, \tag{16}$$

where the notation $Q_{T,mac}$ denotes the macroscopic particle. Is this an experimentally obtainable value? The answer to this is maybe. It depends on what kind of electrodes are being used. Even in vacuum, one cannot increase the strength of

electric field indefinitely without electrical breakdown setting in, beyond which point everything neutralizes.[21] Comparing the two results, Eqs. (15) and (16), $Q_{T,mac}$ is greater than $Q_{T,mic}$ by factor of a million. This result alone shows that the kind of charged-particle oscillation mechanism presented here, i.e., one that does not involve charge transfer processes, is most likely to be observed from microscopic or smaller particles than from macroscopic counterparts.

Because the system illustrated in Fig. 2(a) involves charged-particle executing an oscillatory motion, it radiates electromagnetic energy; and, the power of radiated energy can be obtained from Liénard radiation formula,

$$P_{rad} = \frac{8\pi\varepsilon_0\kappa_3^2 v^2}{3c^3}\left(1-\frac{\dot{z}_d^2}{c^2}\right)^{-3}\ddot{z}_d^2.$$

With the explicit expression for $\ddot{z}_d$ inserted from Eq. (10), this becomes

$$P_{rad} = \frac{8\pi\varepsilon_0\kappa_3^2 v^2}{3c^3}\left(\frac{\pi\varepsilon_0\kappa_3 v}{4m}\left\{\frac{v}{(z_d+b)^2} - \frac{v}{(h-z_d-b)^2} + \frac{\left[\gamma\left(b^3-a^3\right)-b^3\right]E_p}{(z_d+b)^3} + \frac{\left[\gamma\left(b^3-a^3\right)-b^3\right]E_p}{(h-z_d-b)^3} - 8E_p\right\} - g\right)^2. \qquad (17)$$

The profile of Liénard radiation power corresponding to the oscillating core-shell structured charged-particle illustrated in Fig. 6 has been computed using Eq. (17). The result shows train of emitted radiation power as the particle oscillates, as illustrated in Fig. 7.

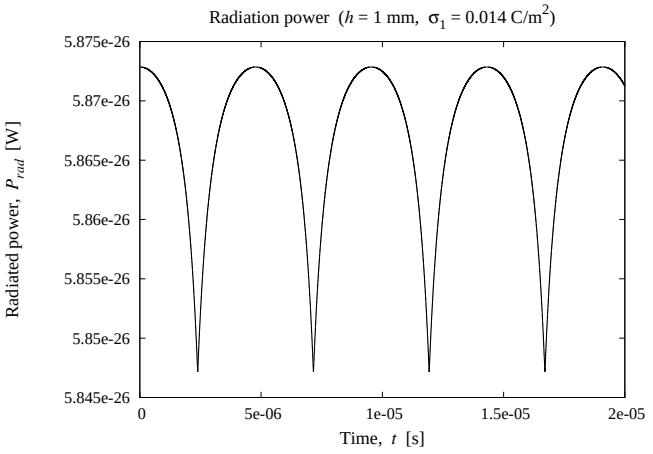

Figure 7: The profile of Liénard radiation power corresponding to the oscillating charged-particle illustrated in Fig. 6.

It is worthwhile to discuss the types of forces involved in the plot of Fig. 6. The force responsible for generating such particle motion is Eq. (8) (or Eq. (9)), of course. Since the force contribution from gravity is negligible in the oscillation regime, I shall only work with $\mathbf{F}_1$ and $\mathbf{F}_2$ of Eqs. (6) and (7), respectively, for the discussion here. The force $\mathbf{F}_1$ is composed of the following three force contributions,

$$\mathbf{F}_1 = \mathbf{f}_{1,1} + \mathbf{f}_{1,2} + \mathbf{f}_{1,3},$$

where

$$\mathbf{f}_{1,1} = \mathbf{e}_z\frac{1}{16}\frac{Q_T v}{s^2},$$
$$\mathbf{f}_{1,2} = \mathbf{e}_z\frac{1}{16}\frac{Q_T\left[\gamma\left(b^3-a^3\right)-b^3\right]}{s^3}E_p,$$
$$\mathbf{f}_{1,3} = -\mathbf{e}_z\frac{Q_T}{4}E_p.$$

From Eqs. (3) and (4), it can be seen that

$$v > 0 \text{ and } 1 > \gamma > 0.$$

This implies, $\gamma\left(b^3-a^3\right)-b^3 < 0$ and the previous forces can be expressed as

$$\mathbf{f}_{1,1} \sim \mathbf{e}_z\frac{1}{s^2},$$
$$\mathbf{f}_{1,2} \sim -\mathbf{e}_z\frac{E_p}{s^3},$$
$$\mathbf{f}_{1,3} \sim -\mathbf{e}_z E_p.$$

Physically, $\mathbf{f}_{1,1}$ represents the force between the charged particle and the image charge formed on the surface of conductor plate. Since the image (or induced) charge has opposite polarity, this force attracts the charged particle towards the plate. And, since $\mathbf{f}_{1,1}$ is in the direction of $\mathbf{e}_z$, this confirms such action. The $\mathbf{f}_{1,3}$ physically represents the force by electric field on the charged particle. Such force always pushes a positively charged particle in the direction of electric field. And, since $\mathbf{f}_{1,3}$ is in the direction of $-\mathbf{e}_z$, which is the direction of electric field, this also confirms such property. The remaining force term, $\mathbf{f}_{1,2}$, is a direct consequence of having a core-shell structured charged-particle. To be more accurate, $\mathbf{f}_{1,2}$ is a consequence of having particle with structure, which is not a "point" particle. Particles with structure can be polarized by applied electric field and such property gives rise to $\mathbf{f}_{1,2}$. Consequently, this force vanishes in the absence of applied electric field. For a positively charged particle, this force is induced in the same direction as the applied electric field.

Similarly, the force $\mathbf{F}_2$ of Eq. (7) can be decomposed into the following three force contributions:

$$\mathbf{F}_2 = \mathbf{f}_{2,1} + \mathbf{f}_{2,2} + \mathbf{f}_{2,3},$$

where

$$\mathbf{f}_{2,1} = -\mathbf{e}_z\frac{1}{16}\frac{Q_T v}{(h-s)^2},$$
$$\mathbf{f}_{2,2} = \mathbf{e}_z\frac{1}{16}\frac{Q_T\left[\gamma\left(b^3-a^3\right)-b^3\right]}{(h-s)^3}E_p,$$
$$\mathbf{f}_{2,3} = -\mathbf{e}_z\frac{Q_T}{4}E_p.$$

Since $\gamma\left(b^3-a^3\right)-b^3<0$, these can be expressed as

$$\mathbf{f}_{2,1}\sim-\mathbf{e}_z\frac{1}{s^2},$$
$$\mathbf{f}_{2,2}\sim-\mathbf{e}_z\frac{E_p}{s^3},$$
$$\mathbf{f}_{2,3}\sim-\mathbf{e}_zE_p.$$

Physically, $\mathbf{f}_{2,1}$ is the force between the image charge and the charged particle. Since $\mathbf{f}_{2,1}$ is the force arising when charged particle is close to the lower conductor plate, this force must be directed towards the lower conductor plate. Since $\mathbf{f}_{2,1}$ is directed in $-\mathbf{e}_z$, this confirms such requirement. The $\mathbf{f}_{2,3}$ is the force on the positively charged particle due to the presence of electric field. Since electric field is in the $-\mathbf{e}_z$ direction, so is $\mathbf{f}_{2,3}$, as it must. Lastly, $\mathbf{f}_{2,2}$ is a consequence of having a charged-particle with structure and not a point particle. Particles with structure can be polarized by applied electric field and such property gives rise to $\mathbf{f}_{2,2}$. Again, this force is always in the direction of applied electric field for a positively charged particle.

So, what is responsible for charged-particle oscillation? The second force, i.e., $\mathbf{F}_2$ of Eq. (7), cannot be responsible for charged-particle oscillation because $\mathbf{f}_{2,1}$, $\mathbf{f}_{2,2}$, and $\mathbf{f}_{2,3}$ are all directed in the $-\mathbf{e}_z$ direction. However, the first force, i.e., $\mathbf{F}_1$ of Eq. (6), can give rise to charged-particle oscillatory modes. This is because force $\mathbf{F}_1$ contains $\mathbf{f}_{1,1}$, which force points in the opposite direction of $\mathbf{f}_{1,2}$ and $\mathbf{f}_{1,3}$. It is this competition between $\mathbf{f}_{1,1}$ and the other forces, i.e., $\mathbf{f}_{1,2}$ and $\mathbf{f}_{1,3}$, that puts core-shell structured charged-particle in an oscillatory motion. Such mechanism is schematically illustrated in Fig. 8. In region A, the dominant force is $\mathbf{f}_{1,2}$ and the magnitude of this force falls off like $\sim 1/s^3$ with distance, s. However, in region B, contributions from $\mathbf{f}_{1,2}$ weakens rapidly with distance and the force is dominated by $\mathbf{f}_{1,1}$, which force's magnitude falls off like $\sim 1/s^2$ with distance. Then, assuming the positively charged core-shell structured particle satisfies the oscillation criterion specified in Eq. (1), the particle cannot escape region B and enter region C, which region contains no oscillation modes and any particles initially in such region ends up sticking to the lower conductor plate, as schematically illustrated in Fig. 8.

That said, a positively charged core-shell structured particle initially in region B (or region A) would oscillate; and, the trace of such oscillatory motion over time would be represented by the path 1 illustrated in Fig. 8. Here, the path 1 represents the plot of $z_d(t)$ versus time graph, where the time parameter is the horizontal axis. On the other hand, the same particle initially in region C would not have any oscillations, but it would follow the trace of the path 2, where the path 2 represents the plot of $z_d(t)$ versus time graph with horizontal axis being the time axis.

The sharp cusp in region A can be explained from the fact that $\mathbf{f}_{1,2}\sim-\left(1/s^3\right)\mathbf{e}_z$ is an extremely short range force. Since the magnitude of such force goes like $\sim 1/s^3$, it can generate very large impulse over short time. Since $\mathbf{f}_{1,2}$ is in $-\mathbf{e}_z$ direction, the particle is repulsed from the surface with very large force occurring over very short period. However, in region B,

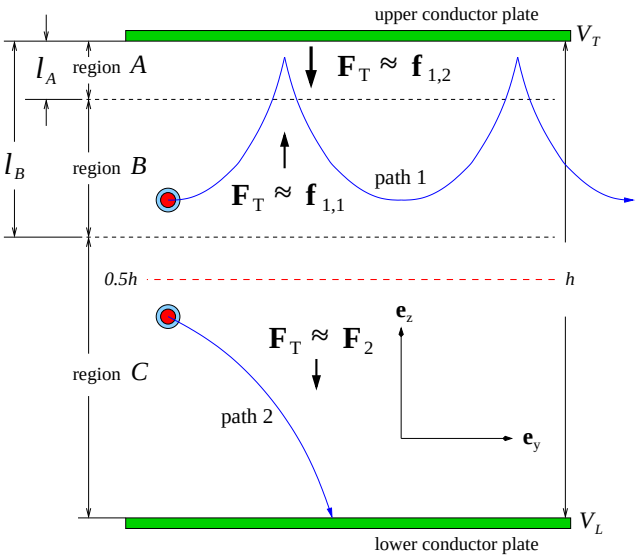

Figure 8: (Color online) Different forces dominate in each regions. In region A, the dominant force is $\mathbf{f}_{1,2}$. In region B, the dominant force is $\mathbf{f}_{1,1}$. In region C, the dominant force is $\mathbf{F}_2$. The path 1 and path 2 represent the plots of $z_d(t)$ versus time graph, where the time parameter is the horizontal axis. Here, $V_T>V_L$.

this force decays extremely rapidly and $\mathbf{f}_{1,1}\sim\left(1/s^2\right)\mathbf{e}_z$ dominates there. The direction of $\mathbf{f}_{1,1}$ is in $\mathbf{e}_z$; hence, the particle is pulled back to the upper conductor plate. This process repeats itself, resulting in an oscillatory motion.

What happens when the magnitude of applied electric field, E_p, is increased? The force $\mathbf{f}_{1,1}\sim\left(1/s^2\right)\mathbf{e}_z$ is independent of E_p; therefore, l_B does not change in Fig. 8. On the other hand, the force $\mathbf{f}_{1,2}\sim-\left(1/s^3\right)\mathbf{e}_z$ has an explicit dependence on the applied electric field, i.e.,

$$\mathbf{f}_{1,2}\sim-\mathbf{e}_z\frac{E_p}{s^3};$$

therefore, the l_A in Fig. 8 gets increased to $l_A+\Delta l_A$ with increased E_p. Here, l_A and l_B represent the locations of borderlines for regions A and B, respectively. The result is that charged-particle trapped inside the region B is now forced to rebound more frequently due to the fact that the width of region B has been decreased by Δl_A. Consequently, the frequency of charged-particle oscillation increases with increased applied electric field; and, this is schematically illustrated in Fig. 9, where it shows that new path 1 has higher frequency than the old path 1. To validate this, Eq. (10) has been plotted using the identical settings used to obtain the result in Fig. 6. This time, however, the strength of applied electric field has been increased from $8\,\mathrm{MV\cdot m^{-1}}$ to $12\,\mathrm{MV\cdot m^{-1}}$. The result is shown in Fig. 10. This result can be compared with the one in Fig. 6, which was obtained for $E_p=8\,\mathrm{MV\cdot m^{-1}}$. For the case of $E_p=12\,\mathrm{MV\cdot m^{-1}}$, the frequency of charged-particle oscillation has been approximately doubled compared to that of the case of $E_p=8\,\mathrm{MV\cdot m^{-1}}$. Notice that although

the oscillation frequency has been approximately doubled, its amplitude has been nearly halved. This must be so because the particle's oscillation frequency had been increased as a result of reduced width of region B (or increased width of region A).

Now, one cannot increase E_p indefinitely to obtain higher oscillation frequencies because, eventually, the width of region B would become zero. And, beyond that point, the charged-particle enters the region C and ends up sticking to the surface of the lower conductor plate. In region C, there are no oscillatory modes so any charged particle in that region gets attracted to the surface of lower conductor plate and stays there indefinitely.

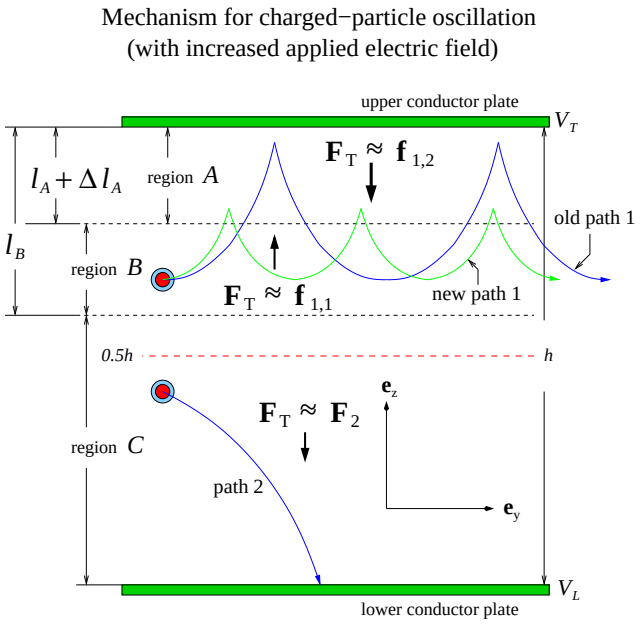

Figure 9: (Color online) The width of region A has been increased to $l_A + \Delta l_A$ as a result of increased strength of applied electric field, $\mathbf{E}_p = -\mathbf{e}_z E_p$. The new path 1, old path 1, and path 2 represent the plots of $z_d(t)$ versus time graph, where the time parameter is the horizontal axis. Here, $V_T > V_L$.

Having explained the kind of forces involved in the charged-particle oscillation, i.e., plots generated in Figs. (6) and (10), it is now clear why there are cusps in the plot. The shape of these sharp turning points can be deceiving because these points are not really what they appear to be. In fact, these turning points are smoothly varying points and this is illustrated in Fig. 11, where one of such sharp points has been enlarged for a view. At these points, the magnitude of force experienced by the particle falls off with distance like $\sim 1/s^3$, where s is the distance between the particle's center of mass and the rebounding plate's surface. At very short separation distances, this repulsion force becomes extremely impulsive over very short period. But, nevertheless, $\sim 1/s^3$ is still a well behaved function because s cannot become zero, as the particle cannot touch the surface of rebounding conductor plate. Doing so would require an infinite energy, which is not possible.

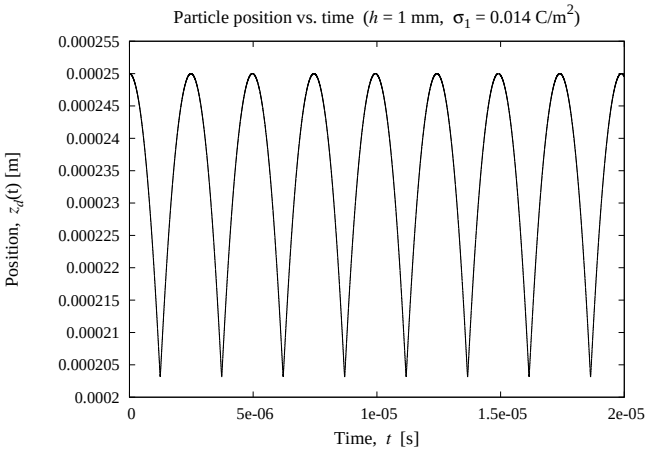

Figure 10: Particle distance from the surface of upper conductor plate as function of time. For the plot, the values defined in Eq. (11) have been used. Here, however, the value of $V_T - V_L$ has been increased to $V_T - V_L = 12\,\mathrm{kV}$, implying an applied electric field strength of $E_p = 12\,\mathrm{MV\cdot m^{-1}}$. The upper electrode is located at $z_d = 0\,\mathrm{m}$.

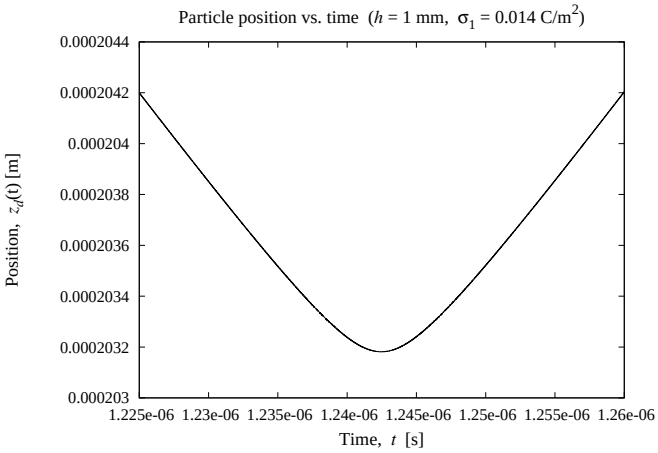

Figure 11: Particle distance from the surface of upper conductor plate as function of time. The first sharp turning point near $z_d \approx 0.000205\,\mathrm{m}$ in Fig. 10 has been enlarged for a view, which shows a smoothly varying curve.

What happens when the core-shell structured particle is negatively charged? In that case, the $\mathbf{F}_1$ and $\mathbf{F}_2$ of Eqs. (6) and (7) get modified as

$$\mathbf{F}_1 = \mathbf{e}_z \frac{|Q_T|}{4}\left[\frac{|v|}{4s^2} + \frac{\left|\gamma\left(b^3-a^3\right)-b^3\right|E_p}{4s^3} + E_p\right]$$

and

$$\mathbf{F}_2 = \mathbf{e}_z \frac{|Q_T|}{4}\left[\frac{\left|\gamma\left(b^3-a^3\right)-b^3\right|E_p}{4\left(h-s\right)^3} - \frac{|v|}{4\left(h-s\right)^2} + E_p\right].$$

To distinguish the analysis here from the previous case involving a positively charged core-shell structured particle, I shall

rewrite $\mathbf{F}_1$ and $\mathbf{F}_2$ as

$$\mathbf{N}_1 = \mathbf{e}_z \frac{|Q_T|}{4}\left[\frac{|\nu|}{4s^2} + \frac{\left|\gamma\left(b^3-a^3\right)-b^3\right|E_p}{4s^3} + E_p\right]$$

and

$$\mathbf{N}_2 = \mathbf{n}_{2,1} + \mathbf{n}_{2,2} + \mathbf{n}_{2,3},$$

where

$$\mathbf{n}_{2,1} = -\mathbf{e}_z \frac{|Q_T|}{16}\frac{|\nu|}{(h-s)^2} \sim -\mathbf{e}_z \frac{1}{(h-s)^2},$$

$$\mathbf{n}_{2,2} = \mathbf{e}_z \frac{|Q_T|}{16}\frac{\left|\gamma\left(b^3-a^3\right)-b^3\right|}{(h-s)^3}E_p \sim \mathbf{e}_z \frac{E_p}{(h-s)^3},$$

$$\mathbf{n}_{2,3} = \mathbf{e}_z \frac{|Q_T|}{4}E_p \sim \mathbf{e}_z E_p.$$

Since all of the terms are positive in force $\mathbf{N}_1$, it cannot generate any oscillations. On the other hand, the force $\mathbf{N}_2$ contains both positive and negative terms; and, therefore, it can generate oscillatory modes. Such is schematically illustrated in Fig. 12.

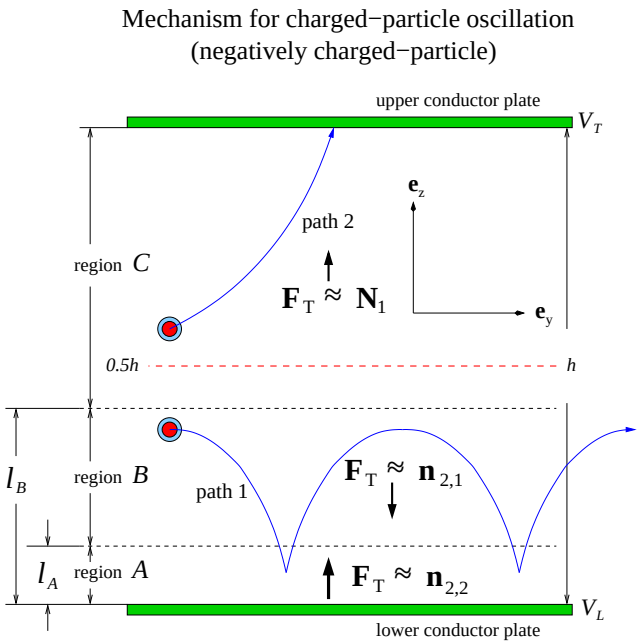

Figure 12: (Color online) For the case of negatively charged-particle, the oscillation modes exist near the lower conductor plate, which is exactly opposite of the positively charged-particle case (see Fig. 8). In region A, the dominant force is $\mathbf{n}_{2,2}$; and, in region B, the dominant force is $\mathbf{n}_{2,1}$. The path 1 and path 2 represent the plots of $z_d(t)$ versus time graph, where the time parameter is the horizontal axis. Here, $V_T > V_L$.

To validate the argument illustrated in Fig. 12, Eq. (10) has been plotted using the same values specified in Eq. (11), except now $\sigma_1 = -0.014\,\mathrm{C\cdot m^{-2}}$. Also, to account for the oscillatory motion, the initial conditions have been specified as

$$z_d(0) = 0.75h \quad \text{and} \quad \dot{z}_d(0) = 0.$$

Such initial conditions have been chosen because oscillatory modes only exist for $z_d > 0.5h$ for negatively charged particles. The result is plotted in Fig. 13, where it shows negatively charged core-shell structured particle oscillating near the lower conductor plate. In the plot, the lower conductor plate is located at $z_d = 0.001\,\mathrm{m}$ and the upper conductor plate is located at $z_d = 0\,\mathrm{m}$. To show that charged-particle trajectory is represented by a well behaved function, one of the sharp turning points in Fig. 13 has been enlarged for inspection. As it can be seen in Fig. 14, the cusp looking points are deceiving because these are smoothly varying points. The magnitude of force acting on the particle near these points falls off with distance like $\sim 1/(h-s)^3$. When the negatively charged core-shell structured particle is very close to the lower conductor plate, $h-s$ becomes very small and this results in a very large force that acts to repulse the particle from the surface of the lower conductor plate. Nonetheless, this is a well defined force because $h-s$ cannot become zero. Doing so would require an infinite energy, which is not possible.

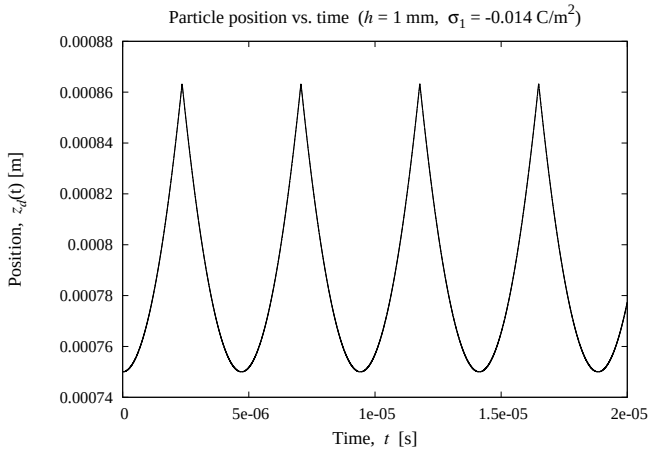

Figure 13: Particle distance from the surface of upper conductor plate as function of time. The lower electrode is located at $z_d = 0.001\,\mathrm{m}$ and the upper electrode is located at $z_d = 0\,\mathrm{m}$. The charged particle is negatively charged and it is oscillating near the lower electrode.

This briefly summarizes the essence of this investigation. To complete the task, I shall now work out the detailed derivations of key solutions used in this article. I shall begin by solving the boundary value problem for the electrostatic potentials in regions M_1, M_2, and M_3 of Fig. 2.

III. THEORY

A. Free charge distribution

The correct specification of electric charge distribution is of crucial importance in any electrostatic boundary value prob-

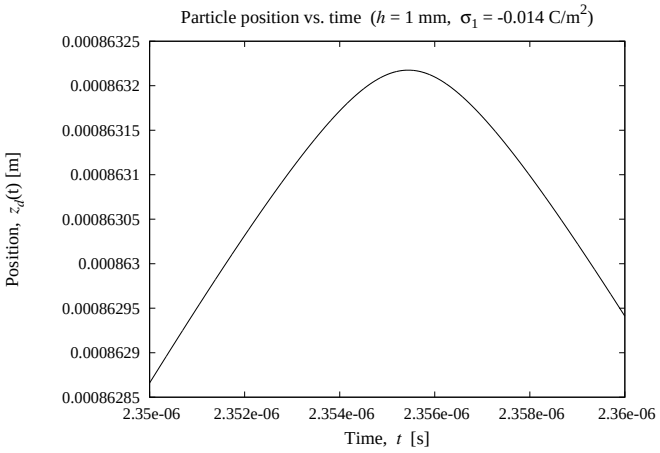

Figure 14: Particle distance from the surface of upper conductor plate as function of time. The first sharp turning point near $z_d \approx 0.00086\,\mathrm{m}$ in Fig. 13 has been enlarged for a view, which shows a smoothly varying curve.

lem. When an uncharged, electrically neutral, spherical conductor is placed in an otherwise uniform electric field, the charges inside the conductor redistribute such that the potential V_1 is a constant there, as illustrated in Fig. 15(a). By definition, in an electrically neutral conductor, every charges are paired with one with opposite polarity. Therefore, the spherical conductor illustrated in Fig. 15(a), as a whole, is electrically neutral.

Now, how do charges get distributed when you place a positively charged spherical conductor in an otherwise uniform, constant, electric field? By definition, an electrically charged conductor has excess number of charges of one polarity that cannot be paired with one with opposite polarity. The paired ones do whatever they can to make net electric field zero inside the conductor. The result is that the paired ones redistribute as illustrated in Fig. 15(a). What about the excess, unpaired, charges of same polarity? These must be redistributed such that the potential V_1 is a constant inside the conductor. One such distribution, perhaps the only one, is illustrated in Fig. 15(b). Assuming the charged spherical conductor has only the surface "free charges" and no volume "free charges," i.e., no excess charges embedded inside the volume, the free charges on the surface of spherical conductor must be uniformly distributed over the entire spherical surface else the net electric field inside the spherical conductor would not be a zero. As an alternate explanation, the spherical conductor in Fig. 15(a), including its surface, represents an equipotential surface. When an excess of free charges of same polarity, say positive charges, is placed on such an equipotential surface, the charges get instantaneously redistributed over the surface due to Coulomb repulsion between the charges. The result is that these charges are uniformly distributed over the equipotential surface, as illustrated in Fig. 15(b).

That explained, I shall assume that surface "free charge" density σ_1 in Fig. 2 is a constant which is uniformly distributed over the surface $r = a$ of the spherical conductor core

(a) Neutral spherical conductor in an otherwise uniform DC electric field **E**

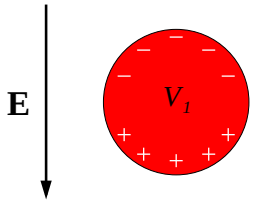

(b) Charged spherical conductor in an otherwise uniform DC electric field **E**

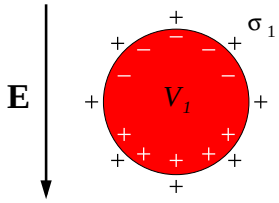

Figure 15: (Color online) Charge distributions of (a) electrically neutral spherical conductor and (b) a positively charged spherical conductor with surface free charge density, σ_1, in an otherwise uniform electric field, $\mathbf{E}_p$.

throughout this work. To generalize the problem, the dielectric shell surrounding the spherical core in Fig. 2 is allowed for a surface "free charge" density σ_2 at $r = b$. Introduction of free charge on the surface of dielectric shell is purely academic. For realistic dielectrics, σ_2 is negligibly small, if not zero. Hence, it can always be set to zero in the final solution. Therefore, I shall keep the problem simple by assuming that σ_2 is a constant which is also uniformly distributed over the surface $r = b$ of the dielectric shell throughout this work.

Lastly, although the illustration in Fig. 15 considered only an excess positive charge case in which $Q_T > 0$, the treatment throughout this work is not limited to such case only. The effective charge Q_T can have either positive or negative polarities.

B. Derivation of electrostatic potentials

The apparatus for the problem is illustrated in Fig. 2(a), where a core-shell structured charged-particle is placed between two DC voltage biased plane-parallel conductors. Electrostatic potentials in regions M_1, M_2, and M_3 are described by Laplace equation,

$$\nabla^2 V = 0.$$

In spherical polar coordinate system, Fig. 2(b), Laplace equation reads

$$\frac{1}{r^2}\frac{\partial}{\partial r}\left(r^2\frac{\partial V}{\partial r}\right)+\frac{1}{r^2\sin\theta}\frac{\partial}{\partial\theta}\left(\sin\theta\frac{\partial V}{\partial\theta}\right)+\frac{1}{r^2\sin^2\theta}\frac{\partial^2 V}{\partial\phi^2}=0.$$

For the system with azimuth symmetry,

$$\frac{\partial V}{\partial\phi}=0,$$

the Laplace equation reduces to

$$\frac{\partial}{\partial r}\left(r^2\frac{\partial V}{\partial r}\right)+\frac{1}{\sin\theta}\frac{\partial}{\partial\theta}\left(\sin\theta\frac{\partial V}{\partial\theta}\right)=0. \tag{18}$$

Equation (18) has the general solution given by

$$V(r,\theta)=\sum_{\ell=0}^{\infty}\left(A_\ell r^\ell+\frac{B_\ell}{r^{\ell+1}}\right)P_\ell,$$

where coefficients A_ℓ and B_ℓ are constants, and $P_\ell\equiv P_\ell(\cos\theta)$ is the Legendre polynomial of order ℓ. For regions M_1, M_2, and M_3 in Fig. 2(a), the electrostatic potentials are given by

$$V_1(r,\theta)=\sum_{\ell=0}^{\infty}A_\ell r^\ell P_\ell, \tag{19}$$

$$V_2(r,\theta)=\sum_{\ell=0}^{\infty}\left(B_\ell r^\ell+\frac{C_\ell}{r^{\ell+1}}\right)P_\ell, \tag{20}$$

$$V_3(r,\theta)=\sum_{\ell=0}^{\infty}\left(D_\ell r^\ell+\frac{E_\ell}{r^{\ell+1}}\right)P_\ell, \tag{21}$$

where coefficients A_ℓ, B_ℓ, C_ℓ, D_ℓ, and E_ℓ are to be joined together by appropriate boundary conditions at the interfaces between regions. Equation (19) does not contain terms like $\sim r^{-\ell-1}$ because these terms blow up at the origin.

Electrostatic potential inside of a conductor is constant; and, therefore, Eq. (19) becomes

$$V_1(r,\theta)=A_0\equiv V_0, \tag{22}$$

where V_0 is a constant. Potential is continuous at $r=a$,

$$V_2(a,\theta)=V_1(a,\theta).$$

From Eqs. (20) and (22), it can be shown that

$$B_0+\frac{C_0}{a}+\sum_{\ell=1}^{\infty}\left(B_\ell a^\ell+\frac{C_\ell}{a^{\ell+1}}\right)P_\ell=V_0$$

or

$$\left(B_0-V_0+\frac{C_0}{a}\right)P_0+\sum_{\ell=1}^{\infty}\left(B_\ell a^\ell+\frac{C_\ell}{a^{\ell+1}}\right)P_\ell=0,$$

where $P_0=1$. It follows that each Legendre polynomials (P_0, P_1, P_2, and so on) are linearly independent functions; and, therefore, the coefficient of each Legendre polynomials must be zero independently else this algebraic equation cannot be satisfied. Thus,

$$B_0+C_0a^{-1}=V_0,$$
$$B_\ell a^\ell+C_\ell a^{-\ell-1}=0.$$

Solving for C_0 and C_ℓ yields

$$C_0=a(V_0-B_0),$$
$$C_\ell=-B_\ell a^{2\ell+1},\quad \ell\geq 1.$$

From these results, Eq. (20) becomes

$$V_2(r,\theta)=B_0\left(1-\frac{a}{r}\right)+\frac{aV_0}{r}+\sum_{\ell=1}^{\infty}B_\ell\left(r^\ell-\frac{a^{2\ell+1}}{r^{\ell+1}}\right)P_\ell. \tag{23}$$

Equations (21) and (23) must be continuous at $r=b$,

$$V_2(b,\theta)=V_3(b,\theta).$$

With Eqs. (21) and (23), it can be shown that

$$B_0\left(1-\frac{a}{b}\right)+\frac{aV_0}{b}+\sum_{\ell=1}^{\infty}B_\ell\left(b^\ell-\frac{a^{2\ell+1}}{b^{\ell+1}}\right)P_\ell=D_0+\frac{E_0}{b}+\sum_{\ell=1}^{\infty}\left(D_\ell b^\ell+\frac{E_\ell}{b^{\ell+1}}\right)P_\ell$$

or

$$0=\left[B_0\left(1-\frac{a}{b}\right)+\frac{aV_0}{b}-D_0-\frac{E_0}{b}\right]P_0+\sum_{\ell=1}^{\infty}\left[B_\ell\left(b^\ell-\frac{a^{2\ell+1}}{b^{\ell+1}}\right)-D_\ell b^\ell-\frac{E_\ell}{b^{\ell+1}}\right]P_\ell,$$

where $P_0=1$. Again, Legendre polynomials (P_0, P_1, P_2, and so on) are linearly independent functions; and, therefore, the coefficient of each Legendre polynomials must vanish independently else this algebraic equation cannot be satisfied. Hence,

$$D_0+\frac{E_0}{b}=B_0\left(1-\frac{a}{b}\right)+\frac{aV_0}{b},$$
$$D_\ell b^\ell+\frac{E_\ell}{b^{\ell+1}}=B_\ell\left(b^\ell-\frac{a^{2\ell+1}}{b^{\ell+1}}\right),$$

and the following coefficients are obtained:

$$E_0=B_0(b-a)+aV_0-D_0b,$$
$$E_\ell=B_\ell\left(b^{2\ell+1}-a^{2\ell+1}\right)-D_\ell b^{2\ell+1},\quad \ell\geq 1.$$

Using these results, Eq. (21) becomes

$$V_3(r,\theta)=D_0\left(1-\frac{b}{r}\right)+\frac{B_0(b-a)+aV_0}{r}+\sum_{\ell=1}^{\infty}\left[D_\ell\left(r^\ell-\frac{b^{2\ell+1}}{r^{\ell+1}}\right)+\frac{B_\ell\left(b^{2\ell+1}-a^{2\ell+1}\right)}{r^{\ell+1}}\right]P_\ell. \tag{24}$$

Equation (24) must simultaneously satisfy the boundary conditions at the surfaces of the upper and the lower conductor plates illustrated in Fig. 2(a).

In Cartesian coordinates, the surface of the upper conductor plate is described by the $z = s$ plane and the surface of the lower conductor plate is described by the $z = s - h$ plane. At distances sufficiently far from the particle (or very close to the surface of conductor plates), the potential inside of the parallel plates can be approximated as

$$V_p = -\int_{s-h}^{z} \mathbf{E}_p \cdot \mathbf{e}_z dz' + V_L,$$

where V_L is the voltage applied to the lower conductor plate, $\mathbf{e}_z$ is the versor along the Cartesian z axis, and $\mathbf{E}_p$ is the electric field inside of the parallel plates in the absence of the charged-particle. The expression for $\mathbf{E}_p$ is given by

$$\mathbf{E}_p = -\mathbf{e}_z \frac{1}{h}\left(V_T - V_L\right), \tag{25}$$

from which the V_p can be obtained:

$$V_p(z) = E_p(z - s + h) + V_L, \tag{26}$$

where

$$E_p \equiv \left\|\mathbf{E}_p\right\| = \frac{1}{h}\left(|V_T - V_L|\right). \tag{27}$$

In spherical polar coordinate system, the Cartesian coordinate z is represented by

$$z = r\cos\theta$$

and Eq. (26) becomes

$$V_p(r,\theta) = E_p(r\cos\theta - s + h) + V_L. \tag{28}$$

For r very large, but not infinite in extent, the contributions from terms like $\sim r^{-1}$ and $\sim r^{-\ell-1}$ become negligible in Eq. (24) and the V_3 takes the form given by

$$V_3(r,\theta) \approx D_0 + \sum_{\ell=1}^{\infty} D_\ell r^\ell P_\ell, \tag{29}$$

where $b \ll r < \infty$. At distances sufficiently far from the particle, $V_3(r,\theta) \approx V_p(r,\theta)$.

One may recall a typical problem in electrodynamics, wherein a charged sphere is immersed in an otherwise constant and uniform electric field. For instance, assuming uniform electric field is along the $\mathbf{e}_z$ axis, a useful boundary condition is that at infinity, electric field is just $\mathbf{E} = \mathbf{e}_z \|\mathbf{E}\| r\cos\theta$. Now, at distances which are infinitesimally close to the conductor plate's surface, electric field must be perpendicular to the plate's surface. This is because the surface of conductor plate is an equipotential surface and electric fields are perpendicular to the equipotential surface by definition, of course. In this regard, Eq. (28) mimics the electric field boundary condition at infinity for the textbook problem in electrodynamics, wherein a charged sphere is immersed in an otherwise constant and uniform electric field and the student is asked to solve for the potential around the sphere.

That said, Eqs. (28) and (29) are equated to yield

$$\begin{aligned} &D_0 + D_1 r\cos\theta + \sum_{\ell=2}^{\infty} D_\ell r^\ell P_\ell \\ &\quad\approx E_p r\cos\theta + E_p(h-s) + V_L. \end{aligned}$$

Matching the coefficients of the like Legendre polynomials yield

$$\begin{aligned} D_0 &\approx E_p(h-s) + V_L, \\ D_1 &\approx E_p, \\ D_\ell &\approx 0, \quad \ell \geq 2. \end{aligned}$$

Using these results, Eq. (24) becomes

$$\begin{aligned} V_3(r,\theta) \approx{}& E_p(h-s) + V_L + E_p r\cos\theta \\ &+ \left[B_0(b-a) + aV_0 - bE_p(h-s) - bV_L\right]\frac{1}{r} \\ &+ \left[B_1\left(b^3 - a^3\right) - b^3 E_p\right]\frac{\cos\theta}{r^2} \\ &+ \sum_{\ell=2}^{\infty} \frac{B_\ell\left(b^{2\ell+1} - a^{2\ell+1}\right)}{r^{\ell+1}} P_\ell, \end{aligned} \tag{30}$$

where it is understood that $b \ll r < \infty$. The electrostatic potential, which satisfies the Laplace equation, is a second order differential equation. Therefore, its derivatives must be satisfied at the boundaries. The remaining unknowns, B_0, B_1, B_ℓ for $\ell \geq 2$, and V_0 are evaluated from the statement about the discontinuity of electric displacement at $r = b$ and at $r = a$.

At $r = b$, the normal component of the electric displacement suffers a discontinuity given by

$$\left[\mathbf{e}_r \cdot \mathbf{D}_3(r,\theta) - \mathbf{e}_r \cdot \mathbf{D}_2(r,\theta)\right]\big|_{r=b} = \sigma_2, \tag{31}$$

where σ_2 is the surface free-charge density at $r = b$, the $\mathbf{e}_r$ is a unit vector pointing in the radially outward direction, and $\mathbf{D}_2$ and $\mathbf{D}_3$ represent electric displacements in regions M_2 and M_3, respectively. In the linear dielectric approximation, the electric displacement can be expressed as

$$\mathbf{D}_i(r,\theta) = -\varepsilon_0 \kappa_i \nabla V_i(r,\theta), \tag{32}$$

where κ_i is the dielectric constant in region M_i and ε_0 is the electric permittivity of the free space. Hence, Eq. (31) can be expressed as

$$\left[\kappa_2 \mathbf{e}_r \cdot \nabla V_2(r,\theta) - \kappa_3 \mathbf{e}_r \cdot \nabla V_3(r,\theta)\right]\big|_{r=b} = \frac{\sigma_2}{\varepsilon_0}. \tag{33}$$

In spherical polar coordinate system, the ∇ operator is defined by

$$\nabla = \mathbf{e}_r \frac{\partial}{\partial r} + \mathbf{e}_\theta \frac{1}{r}\frac{\partial}{\partial\theta} + \mathbf{e}_\phi \frac{1}{r\sin\theta}\frac{\partial}{\partial\phi}$$

and Eq. (33) becomes

$$\left[\kappa_2 \frac{\partial V_2(r,\theta)}{\partial r} - \kappa_3 \frac{\partial V_3(r,\theta)}{\partial r}\right]\Bigg|_{r=b} = \frac{\sigma_2}{\varepsilon_0}, \tag{34}$$

which constitutes the Neumann boundary condition at $r=b$. In explicit forms, the derivatives in Eq. (34) are evaluated as

$$\frac{\partial V_2(r,\theta)}{\partial r} = (B_0 - V_0)\frac{a}{r^2} + \sum_{\ell=1}^{\infty} B_\ell \left[\ell r^{\ell-1} + \frac{(\ell+1)a^{2\ell+1}}{r^{\ell+2}}\right] P_\ell \tag{35}$$

and

$$\begin{aligned}\frac{\partial V_3(r,\theta)}{\partial r} &= E_p\cos\theta \\ &- \left[B_0(b-a) + aV_0 - bE_p(h-s) - bV_L\right]\frac{1}{r^2} \\ &- 2\left[B_1\left(b^3-a^3\right) - b^3E_p\right]\frac{\cos\theta}{r^3} \\ &- \sum_{\ell=2}^{\infty}\frac{(\ell+1)B_\ell\left(b^{2\ell+1}-a^{2\ell+1}\right)}{r^{\ell+2}}P_\ell,\end{aligned} \tag{36}$$

where Eqs. (23) and (30) have been used. Insertion of Eqs. (35) and (36) into Eq. (34) yields

$$\begin{aligned}\frac{\sigma_2}{\varepsilon_0} &= \frac{1}{b^2}\left\{B_0\left[a(\kappa_2-\kappa_3)+b\kappa_3\right]\right. \\ &\left. -a(\kappa_2-\kappa_3)V_0 - b\kappa_3E_p(h-s) - b\kappa_3V_L\right\} \\ &+ \kappa_2\left(1+\frac{2a^3}{b^3}\right)B_1\cos\theta \\ &+ \kappa_3\left\{\frac{2}{b^3}\left[B_1\left(b^3-a^3\right)-b^3E_p\right]-E_p\right\}\cos\theta \\ &+ \sum_{\ell=2}^{\infty}B_\ell P_\ell\left\{\frac{\kappa_2\ell}{b^{1-\ell}}\right. \\ &\left. +\frac{\ell+1}{b^{\ell+2}}\left[a^{2\ell+1}(\kappa_2-\kappa_3)+b^{2\ell+1}\kappa_3\right]\right\}\end{aligned}$$

or

$$\begin{aligned}0 &= \left(\frac{1}{b^2}\left\{B_0\left[a(\kappa_2-\kappa_3)+b\kappa_3\right] - b\kappa_3V_L\right.\right. \\ &\left.\left. -a(\kappa_2-\kappa_3)V_0 - b\kappa_3E_p(h-s)\right\} - \frac{\sigma_2}{\varepsilon_0}\right)P_0 \\ &+ \kappa_2\left(1+\frac{2a^3}{b^3}\right)B_1P_1 \\ &+ \kappa_3\left\{\frac{2}{b^3}\left[B_1\left(b^3-a^3\right)-b^3E_p\right]-E_p\right\}P_1 \\ &+ \sum_{\ell=2}^{\infty}B_\ell P_\ell\left\{\frac{\kappa_2\ell}{b^{1-\ell}}\right. \\ &\left. +\frac{\ell+1}{b^{\ell+2}}\left[a^{2\ell+1}(\kappa_2-\kappa_3)+b^{2\ell+1}\kappa_3\right]\right\},\end{aligned}$$

where $P_0=1$ and $P_1=\cos\theta$. Because each Legendre polynomials of order ℓ are linearly independent functions, this algebraic relation can be satisfied if and only if the coefficients of each Legendre polynomials vanish independently. Hence,

$$\begin{aligned}&B_0\left[a(\kappa_2-\kappa_3)+b\kappa_3\right] - a(\kappa_2-\kappa_3)V_0 \\ &-b\kappa_3\left[E_p(h-s)+V_L\right] - \frac{b^2\sigma_2}{\varepsilon_0} = 0,\end{aligned}$$

$$\begin{aligned}&\kappa_3\left\{\frac{2}{b^3}\left[B_1\left(b^3-a^3\right)-b^3E_p\right]-E_p\right\} \\ &+\kappa_2\left(1+\frac{2a^3}{b^3}\right)B_1 = 0,\end{aligned}$$

and

$$B_\ell\left\{\frac{\ell+1}{b^{\ell+2}}\left[a^{2\ell+1}(\kappa_2-\kappa_3)+b^{2\ell+1}\kappa_3\right]+\frac{\kappa_2\ell}{b^{1-\ell}}\right\} = 0.$$

One reads off immediately that

$$\begin{aligned}B_0 &= \frac{b\kappa_3\left[E_p(h-s)+V_L\right]+b^2\varepsilon_0^{-1}\sigma_2}{a(\kappa_2-\kappa_3)+b\kappa_3} \\ &+ \frac{a(\kappa_2-\kappa_3)V_0}{a(\kappa_2-\kappa_3)+b\kappa_3},\end{aligned} \tag{37}$$

$$B_1 = \frac{3\kappa_3b^3E_p}{(\kappa_2+2\kappa_3)b^3+2(\kappa_2-\kappa_3)a^3}, \tag{38}$$

and

$$B_\ell = 0 \ \text{ for } \ \ell\geq 2. \tag{39}$$

With coefficients B_0, B_1, and $B_{\ell\geq 2}$ defined, Eqs. (23) and (30) become

$$\begin{aligned}V_2(r,\theta) &\approx B_0\left(1-\frac{a}{r}\right)+\frac{aV_0}{r} \\ &+ B_1\left(1-\frac{a^3}{r^3}\right)r\cos\theta\end{aligned} \tag{40}$$

and

$$\begin{aligned}V_3(r,\theta) &\approx E_p(h-s)+V_L+E_pr\cos\theta \\ &+ \left[B_0(b-a)+aV_0-bE_p(h-s)-bV_L\right]\frac{1}{r} \\ &+ \left[B_1\left(b^3-a^3\right)-b^3E_p\right]\frac{\cos\theta}{r^2},\end{aligned} \tag{41}$$

where V_0 is the only unknown.

The V_0 is evaluated from the statement about the discontinuity of electric displacement at $r=a$. At $r=a$, the normal component of the electric displacement suffers a discontinuity given by

$$\left[\mathbf{e}_r\cdot\mathbf{D}_2(r,\theta)-\mathbf{e}_r\cdot\mathbf{D}_1(r,\theta)\right]\big|_{r=a} = \sigma_1, \tag{42}$$

where σ_1 is the surface free-charge density at $r=a$ and $\mathbf{D}_1$ is the electric displacement in region M_1. Repeating the same procedure outlined from Eq. (31) through Eq. (34), it can be shown that

$$\left[\kappa_1\frac{\partial V_1(r,\theta)}{\partial r}-\kappa_2\frac{\partial V_2(r,\theta)}{\partial r}\right]\Bigg|_{r=a} = \frac{\sigma_1}{\varepsilon_0}.$$

Since region M_1 is a conductor,

$$\frac{\partial V_1(r,\theta)}{\partial r} = 0$$

and Neumann boundary condition at $r=a$ becomes

$$\left.\frac{\partial V_2(r,\theta)}{\partial r}\right|_{r=a} = -\frac{\sigma_1}{\varepsilon_0\kappa_2}. \tag{43}$$

Using the results in Eqs. (37), (38), and (39), the derivative in Eq. (43) is readily computed from Eq. (35),

$$\frac{\partial V_2(r,\theta)}{\partial r} = (B_0 - V_0)\frac{a}{r^2} + B_1\left(1+\frac{2a^3}{r^3}\right)\cos\theta.$$

With this result, Eq. (43) becomes

$$\frac{B_0 - V_0}{a} + 3B_1\cos\theta = -\frac{\sigma_1}{\varepsilon_0\kappa_2}. \tag{44}$$

The $\cos\theta$ in Eq. (44) can be eliminated by integrating both sides over the spherical surface at $r=a$,

$$\int_{\theta=0}^{\pi}\int_{\phi=0}^{2\pi}\left(\frac{B_0-V_0}{a}+3B_1\cos\theta\right)a^2\sin\theta\, d\theta d\phi = -\int_{\theta=0}^{\pi}\int_{\phi=0}^{2\pi}\frac{\sigma_1}{\varepsilon_0\kappa_2}a^2\sin\theta\, d\theta d\phi,$$

yielding

$$B_0 - V_0 = -\frac{a\sigma_1}{\varepsilon_0\kappa_2}. \tag{45}$$

What I have just done here only surmounts to the computing of total free charge on the sphere of radius $r=a$. For instance, in Eq. (44), one can integrate both sides over the surface $r=a$ of a sphere. The right hand side yields total free charge on the surface $r=a$, ignoring the extra constant factor. The left hand side yields terms with $\cos\theta$ eliminated, as this term has been integrated over. Canceling out the common terms yields Eq. (45).

That explained, B_0 is inserted from Eq. (37) into Eq. (45) to solve for V_0; and, this yields

$$V_0 = V_L + \frac{a(b-a)\sigma_1}{b\varepsilon_0\kappa_2} + \frac{a^2\sigma_1+b^2\sigma_2}{b\varepsilon_0\kappa_3} + E_p(h-s). \tag{46}$$

With Eq. (46), the coefficient B_0 of Eq. (37) becomes

$$B_0 = V_L + \frac{a(2b-a)\sigma_1}{b\varepsilon_0\kappa_2} + \frac{a^2\sigma_1+b^2\sigma_2}{b\varepsilon_0\kappa_3} + E_p(h-s). \tag{47}$$

With coefficients B_1, V_0, and B_0 defined respectively in Eqs. (38), (46), and (47), the electrostatic potentials for regions M_1, M_2, and M_3 are obtained from Eqs. (22), (40), and (41). They are

$$V_1 = V_L + \alpha + E_p(h-s), \quad r\le a, \tag{48}$$

$$V_2(r,\theta) = V_L + \beta + E_p(h-s+\gamma r\cos\theta) - \frac{\lambda}{r} - \frac{a^3\gamma E_p\cos\theta}{r^2}, \quad a<r\le b, \tag{49}$$

and

$$V_3(r,\theta) = V_L + E_p(h-s+r\cos\theta) + \frac{\nu}{r} + \frac{\left[\gamma\left(b^3-a^3\right)-b^3\right]E_p\cos\theta}{r^2} + C, \quad r>b, \tag{50}$$

where α, β, γ, λ, and ν are defined as

$$\begin{aligned}
\alpha &= \frac{a(b-a)\sigma_1}{b\varepsilon_0\kappa_2} + \frac{a^2\sigma_1+b^2\sigma_2}{b\varepsilon_0\kappa_3},\\
\beta &= \frac{a(2b-a)\sigma_1}{b\varepsilon_0\kappa_2} + \frac{a^2\sigma_1+b^2\sigma_2}{b\varepsilon_0\kappa_3},\\
\gamma &= \frac{3\kappa_3 b^3}{(\kappa_2+2\kappa_3)b^3+2(\kappa_2-\kappa_3)a^3},\\
\lambda &= \frac{a^2\sigma_1}{\varepsilon_0\kappa_2},\\
\nu &= \frac{2a(b-a)\sigma_1}{\varepsilon_0\kappa_2} + \frac{a^2\sigma_1+b^2\sigma_2}{\varepsilon_0\kappa_3}.
\end{aligned} \tag{51}$$

For all of the treatment hereafter, only the derivatives of V_3, in particular, the normal derivatives associated with the plane-parallel plate electrodes, are of importance. Therefore, the explicit expression for the constant C in Eq. (50) is not of much concern here.

C. Induced surface charges on conductor plates

In spherical polar coordinate system, ∇ operator is defined by

$$\nabla = \mathbf{e}_r\frac{\partial}{\partial r} + \mathbf{e}_\theta\frac{1}{r}\frac{\partial}{\partial\theta} + \mathbf{e}_\phi\frac{1}{r\sin\theta}\frac{\partial}{\partial\phi},$$

where

$$\begin{aligned}
\mathbf{e}_r &= \mathbf{e}_x\sin\theta\cos\phi + \mathbf{e}_y\sin\theta\sin\phi + \mathbf{e}_z\cos\theta,\\
\mathbf{e}_\theta &= \mathbf{e}_x\cos\theta\cos\phi + \mathbf{e}_y\cos\theta\sin\phi - \mathbf{e}_z\sin\theta,\\
\mathbf{e}_\phi &= -\mathbf{e}_x\sin\phi + \mathbf{e}_y\cos\phi.
\end{aligned}$$

Hence, the $\mathbf{e}_z$ component of ∇ operator is given by

$$\mathbf{e}_z(\mathbf{e}_z\cdot\nabla) = \mathbf{e}_z\cos\theta\frac{\partial}{\partial r} - \mathbf{e}_z\frac{\sin\theta}{r}\frac{\partial}{\partial\theta}.$$

Using the form defined in Eq. (32), the electric displacement in region M_3 is given by

$$\mathbf{D}_3(r,\theta) = -\varepsilon_0\kappa_3\nabla V_3(r,\theta).$$

The $\mathbf{e}_z$ component of $\mathbf{D}_3(r,\theta)$ is obtained by replacing the ∇ with the $\mathbf{e}_z(\mathbf{e}_z\cdot\nabla)$ operator and this gives

$$\mathbf{D}_{3;z}(r,\theta) = \varepsilon_0\kappa_3\mathbf{e}_z\left[\frac{\sin\theta}{r}\frac{\partial V_3(r,\theta)}{\partial\theta} - \cos\theta\frac{\partial V_3(r,\theta)}{\partial r}\right],$$

where the notation $\mathbf{D}_{3;z}(r,\theta)$ denotes the $\mathbf{e}_z$ component of $\mathbf{D}_3(r,\theta)$. With $V_3(r,\theta)$ of Eq. (50), the $\mathbf{e}_z$ component of electric displacement in region M_3 is given by

$$\mathbf{D}_{3;z}(r,\theta)=\varepsilon_0\kappa_3\mathbf{e}_z\left\{\frac{\nu}{r^2}\cos\theta\right.$$
$$\left.+\frac{\left[\gamma\left(b^3-a^3\right)-b^3\right]E_p}{r^3}\left(3\cos^2\theta-1\right)-E_p\right\}. \qquad (52)$$

The surface of the upper conductor plate is described by the Cartesian $z=s$ plane. In the spherical polar coordinate system, the surface of the upper conductor plate is described by

$$\cos\theta=\frac{s}{\sqrt{x^2+y^2+s^2}}.$$

Insertion of the expression for $\cos\theta$ into Eq. (52) yields

$$\mathbf{D}_{3;z}(x,y,s)=\mathbf{e}_z\varepsilon_0\kappa_3\left\{\frac{3\left[\gamma\left(b^3-a^3\right)-b^3\right]E_p s^2}{\left(x^2+y^2+s^2\right)^{5/2}}\right.$$
$$\left.+\frac{\nu s-\left[\gamma\left(b^3-a^3\right)-b^3\right]E_p}{\left(x^2+y^2+s^2\right)^{3/2}}-E_p\right\}. \qquad (53)$$

At the surface of the upper conductor plate, the electric displacement suffers a discontinuity given by

$$\mathbf{e}_z\cdot\mathbf{D}_{ucp;z}(x,y,s)-\mathbf{e}_z\cdot\mathbf{D}_{3;z}(x,y,s)=\sigma_{iup}, \qquad (54)$$

where σ_{iup} is the induced surface charge density on the surface of the upper conductor plate and $\mathbf{D}_{ucp;z}$ is the $\mathbf{e}_z$ component of the electric displacement inside of the upper conductor plate. Since the electric displacement inside of the upper conductor plate is zero, Eq. (54) reduces to

$$\mathbf{e}_z\cdot\mathbf{D}_{3;z}(x,y,s)=-\sigma_{iup}$$

and the surface charge density is given by

$$\sigma_{iup}=-\varepsilon_0\kappa_3\left\{\frac{3\left[\gamma\left(b^3-a^3\right)-b^3\right]E_p s^2}{\left(x^2+y^2+s^2\right)^{5/2}}\right.$$
$$\left.+\frac{\nu s-\left[\gamma\left(b^3-a^3\right)-b^3\right]E_p}{\left(x^2+y^2+s^2\right)^{3/2}}-E_p\right\}, \qquad (55)$$

where Eq. (53) has been inserted for $\mathbf{D}_{3;z}(x,y,s)$.

The surface of the lower conductor plate is described by the Cartesian $z=s-h$ plane. In the spherical polar coordinate system, the surface of the lower conductor plate is given by

$$\cos\theta=\frac{s-h}{\sqrt{x^2+y^2+(s-h)^2}}$$

and Eq. (52) becomes

$$\mathbf{D}_{3;z}(x,y,s-h)$$
$$=\mathbf{e}_z\varepsilon_0\kappa_3\left\{\frac{3\left[\gamma\left(b^3-a^3\right)-b^3\right]E_p(s-h)^2}{\left[x^2+y^2+(s-h)^2\right]^{5/2}}\right.$$
$$\left.+\frac{\nu(s-h)-\left[\gamma\left(b^3-a^3\right)-b^3\right]E_p}{\left[x^2+y^2+(s-h)^2\right]^{3/2}}-E_p\right\}. \qquad (56)$$

At the surface of the lower conductor plate, the electric displacement suffers a discontinuity given by

$$\mathbf{e}_z\cdot\mathbf{D}_{3;z}(x,y,s-h)-\mathbf{e}_z\cdot\mathbf{D}_{lcp;z}(x,y,s-h)=\sigma_{ilp}, \qquad (57)$$

where σ_{ilp} is the induced surface charge density on the surface of the lower conductor plate and $\mathbf{D}_{lcp;z}$ is the $\mathbf{e}_z$ component of the electric displacement inside of the lower conductor plate. Since the electric displacement inside of the lower conductor plate is zero, Eq. (57) reduces to

$$\mathbf{e}_z\cdot\mathbf{D}_{3;z}(x,y,s-h)=\sigma_{ilp}$$

and, with Eq. (56) inserted for $\mathbf{D}_{3;z}(x,y,s-h)$, the induced surface charge density is given by

$$\sigma_{ilp}=\varepsilon_0\kappa_3\left\{\frac{3\left[\gamma\left(b^3-a^3\right)-b^3\right]E_p(h-s)^2}{\left[x^2+y^2+(h-s)^2\right]^{5/2}}\right.$$
$$\left.-\frac{\nu(h-s)+\left[\gamma\left(b^3-a^3\right)-b^3\right]E_p}{\left[x^2+y^2+(h-s)^2\right]^{3/2}}-E_p\right\}, \qquad (58)$$

where $(s-h)$ has been re-expressed as $-(h-s)$ purely for convenience.

In the limit the parallel plates become infinite in extent, the total of induced charges on the surfaces of each conductor plates must add up to the total charge carried by the particle. To check on this, Eqs. (55) and (58) are integrated over the surfaces of infinite parallel conductor plates with gap h. For convenience, I shall perform the integral in the polar coordinate system. In terms of the polar coordinates, Eqs. (55) and (58) become

$$\sigma_{iup}(\rho,s)=-\varepsilon_0\kappa_3\left\{\frac{3\left[\gamma\left(b^3-a^3\right)-b^3\right]E_p s^2}{\left(\rho^2+s^2\right)^{5/2}}\right.$$
$$\left.+\frac{\nu s-\left[\gamma\left(b^3-a^3\right)-b^3\right]E_p}{\left(\rho^2+s^2\right)^{3/2}}-E_p\right\} \qquad (59)$$

and

$$\sigma_{ilp}(\rho,s)=\varepsilon_0\kappa_3\left\{\frac{3\left[\gamma\left(b^3-a^3\right)-b^3\right]E_p(h-s)^2}{\left[\rho^2+(h-s)^2\right]^{5/2}}\right.$$
$$\left.-\frac{\nu(h-s)+\left[\gamma\left(b^3-a^3\right)-b^3\right]E_p}{\left[\rho^2+(h-s)^2\right]^{3/2}}-E_p\right\}, \qquad (60)$$

where $\rho\equiv\sqrt{x^2+y^2}$. Since the surface in polar coordinate system is symmetric about its axis, the total induced charges on both conductors can be performed as follow:

$$Q_{iT}=Q_{iup}+Q_{ilp}$$
$$=\int_{\phi=0}^{2\pi}\int_{\rho=0}^{\infty}\left[\sigma_{iup}(\rho,s)+\sigma_{ilp}(\rho,s)\right]\rho d\rho d\phi$$
$$=2\pi\int_{\rho=0}^{\infty}\left[\sigma_{iup}(\rho,s)+\sigma_{ilp}(\rho,s)\right]\rho d\rho,$$

where Q_{iup} and Q_{ilp} are respectively the total induced charge on the surface of the upper and the lower conductor plates. With Eqs. (59) and (60), the Q_{iT} becomes

$$\frac{Q_{iT}}{\pi\varepsilon_0\kappa_3} = -2\int_0^\infty \left\{ \frac{3\left[\gamma\left(b^3-a^3\right)-b^3\right]E_p s^2}{\left(\rho^2+s^2\right)^{5/2}} - \frac{3\left[\gamma\left(b^3-a^3\right)-b^3\right]E_p (h-s)^2}{\left[\rho^2+(h-s)^2\right]^{5/2}} + \frac{\nu s-\left[\gamma\left(b^3-a^3\right)-b^3\right]E_p}{\left(\rho^2+s^2\right)^{3/2}} + \frac{\nu(h-s)+\left[\gamma\left(b^3-a^3\right)-b^3\right]E_p}{\left[\rho^2+(h-s)^2\right]^{3/2}} \right\} \rho d\rho. \quad (61)$$

Equation (61) involves the following integral types:

$$\int_0^\infty \frac{\rho d\rho}{\left(\rho^2+c^2\right)^{3/2}} = -\frac{1}{\sqrt{\rho^2+c^2}}\bigg|_0^\infty = \frac{1}{c}, \quad (62)$$

$$\int_0^\infty \frac{\rho d\rho}{\left(\rho^2+c^2\right)^{5/2}} = -\frac{1}{3\left(\rho^2+c^2\right)^{3/2}}\bigg|_0^\infty = \frac{1}{3c^3}. \quad (63)$$

With the integral formulas of Eqs. (62) and (63), the Q_{iT} of Eq. (61) is integrated to yield

$$Q_{iT} = -4\pi\varepsilon_0\kappa_3\nu.$$

Insertion of the explicit expression for ν from Eq. (51) yields

$$Q_{iT} = -\left(Q_b+Q_1+Q_2\right), \quad (64)$$

where

$$Q_b = 8\pi a(b-a)\sigma_1\frac{\kappa_3}{\kappa_2},$$
$$Q_1 = 4\pi a^2\sigma_1,$$
$$Q_2 = 4\pi b^2\sigma_2.$$

The three quantities are identified as follow. The Q_1 and Q_2 are the "free charges" on the surfaces at $r=a$ and $r=b$, respectively. The Q_b is the charge contribution arising from the presence of a dielectric shell surrounding the metallic core. This contribution vanishes in the absence of free charge on metallic core (i.e., $\sigma_1=0$) or dielectric shell (i.e., $b-a=0$).

D. Particle dynamics

Two major electrostatic forces are acting on the core-shell structured charged-particle in Fig. 2. One such force is the electrostatic force between the induced charges on the surface of the upper electrode plate and the charged-particle. This force is denoted by $\mathbf{F}_1$. The other force is the electrostatic force arising between the induced charges on the surface of the lower electrode plate and the charged-particle and this force is denoted as $\mathbf{F}_2$. The net force exerted on the charged-particle by induced charges on each surfaces of the conductor plates is therefore given by

$$\mathbf{F} = \mathbf{F}_1+\mathbf{F}_2 = -\frac{1}{2}Q_T\left(\int_{S_1} d\mathbf{E}_1+\int_{S_2} d\mathbf{E}_2\right), \quad (65)$$

where Q_T is the effective charge carried by the charged-particle and $d\mathbf{E}_1$ and $d\mathbf{E}_2$ are respective differential electric fields corresponding to the upper and lower electrode plate surfaces S_1 and S_2, respectively. For instance, $d\mathbf{E}_1$ is the differential electric field associated with the induced surface charge at location $\mathbf{R}_1$ in Fig. 2(a). Similarly, $d\mathbf{E}_2$ is the differential electric field associated with the induced surface charge at location $\mathbf{R}_2$ of Fig. 2(a).

The presence of extra factor of $1/2$, the negative sign, and the exact form of Q_T in Eq. (65) can be explained as follow. The extra factor of $1/2$ in Eq. (65) comes from the fact that each parallel conductor plates sees only an hemisphere of the charged-particle. The effective charge carried by the particle is identical in magnitude to the Q_{iT} of Eq. (64), but with opposite charge polarity. Thus,

$$Q_T = -Q_{iT}$$

or

$$Q_T = 8\pi a(b-a)\sigma_1\frac{\kappa_3}{\kappa_2}+4\pi\left(a^2\sigma_1+b^2\sigma_2\right). \quad (66)$$

The negative sign in Eq. (65) is necessary for specifying correctly the direction of the forces exerted on the core-shell structured charge-particle by induced surface charges from each parallel conductor plates. To demonstrate this, the integrals in Eq. (65) can be represented by

$$\int_{S_i} d\mathbf{E}_i \;\rightarrow\; \frac{1}{4\pi\varepsilon_3}\int_{\phi_i=0}^{2\pi}\int_{\rho_i=0}^{\rho}\frac{\varsigma_i\mathbf{R}_i\rho_i d\rho_i d\phi_i}{\left(\mathbf{R}_i\cdot\mathbf{R}_i\right)^{3/2}}, \quad (67)$$

where ς_i is the induced surface charge at location $\mathbf{R}_i$ (i.e., $i=1,2$) in Fig. 2(a). Now, suppose if ς_1 is positive, then the direction of $d\mathbf{E}_1$ must be in $-\mathbf{R}_1$, as it can be inspected from Fig. 2(a). On the other hand, if ς_1 is negative, then the direction of $d\mathbf{E}_1$ must be in $\mathbf{R}_1$. The same argument can be said for those involving ς_2, $d\mathbf{E}_2$, and $\mathbf{R}_2$. And, this explains the presence of negative sign in Eq. (65).

That said, using the form defined in Eq. (67), the force expression of Eq. (65) becomes

$$\mathbf{F}_i = -\frac{Q_T}{8\pi\varepsilon_3}\int_{\phi_i=0}^{2\pi}\int_{\rho_i=0}^{\rho}\frac{\varsigma_i\mathbf{R}_i\rho_i d\rho_i d\phi_i}{\left(\mathbf{R}_i\cdot\mathbf{R}_i\right)^{3/2}}, \quad (68)$$

where $i=(1,2)$, $\varsigma_1\equiv\sigma_{iup}$ of Eq. (59), $\varsigma_2\equiv\sigma_{ilp}$ of Eq. (60), and ε_3 is the electric permittivity of the region M_3. The explicit expression for $\mathbf{R}_i$, which defines the position of the ς_i

associated with dS_i as illustrated in Fig. 2(a) for $i=(1,2)$, are given by

$$\mathbf{R}_1 = \mathbf{e}_x\rho_1\cos\phi_1 + \mathbf{e}_y\rho_1\sin\phi_1 + \mathbf{e}_z s, \tag{69}$$

$$\mathbf{R}_2 = \mathbf{e}_x\rho_2\cos\phi_2 + \mathbf{e}_y\rho_2\sin\phi_2 + \mathbf{e}_z(s-h), \tag{70}$$

where $h>s$.

The force exerted on the particle by the induced charge on the surface of the upper conductor plate is obtained by inserting $\mathbf{R}_1$ of Eq. (69) into Eq. (68). This yields

$$\mathbf{F}_1 = -\frac{Q_T}{8\pi\varepsilon_3}\int_{\phi_1=0}^{2\pi}\int_{\rho_1=0}^{\rho}\left[\mathbf{e}_x\frac{\varsigma_1\rho_1\cos\phi_1}{\left(\rho_1^2+s^2\right)^{3/2}} + \mathbf{e}_y\frac{\varsigma_1\rho_1\sin\phi_1}{\left(\rho_1^2+s^2\right)^{3/2}} + \mathbf{e}_z\frac{\varsigma_1 s}{\left(\rho_1^2+s^2\right)^{3/2}}\right]\rho_1 d\rho_1 d\phi_1. \tag{71}$$

The two terms in the integrand with $\cos\phi_1$ and $\sin\phi_1$ vanish when integrated over $d\phi$. Thus, Eq. (71) reduces to

$$\mathbf{F}_1 = -\mathbf{e}_z\frac{Q_T s}{4\varepsilon_3}\int_0^{\rho}\frac{\sigma_{iup}\rho_1 d\rho_1}{\left(\rho_1^2+s^2\right)^{3/2}}, \tag{72}$$

where $\varsigma_1 \equiv \sigma_{iup}$. Insertion of the explicit expression for σ_{iup} from Eq. (59) into Eq. (72) yields

$$\mathbf{F}_1 = \mathbf{e}_z\frac{Q_T s}{4}\int_0^{\rho}\left\{\frac{3\left[\gamma\left(b^3-a^3\right)-b^3\right]E_p s^2}{\left(\rho_1^2+s^2\right)^4} + \frac{\nu s-\left[\gamma\left(b^3-a^3\right)-b^3\right]E_p}{\left(\rho_1^2+s^2\right)^3} - \frac{E_p}{\left(\rho_1^2+s^2\right)^{3/2}}\right\}\rho_1 d\rho_1. \tag{73}$$

Equation (73) involves the following type of integrals:

$$\int_0^{\rho}\frac{\rho_1 d\rho_1}{\left(\rho_1^2+s^2\right)^4} = \frac{1}{6s^6} - \frac{1}{6\left(\rho^2+s^2\right)^3}, \tag{74}$$

$$\int_0^{\rho}\frac{\rho_1 d\rho_1}{\left(\rho_1^2+s^2\right)^3} = \frac{1}{4s^4} - \frac{1}{4\left(\rho^2+s^2\right)^2}, \tag{75}$$

$$\int_0^{\rho}\frac{\rho_1 d\rho_1}{\left(\rho_1^2+s^2\right)^{3/2}} = \frac{1}{s} - \frac{1}{\sqrt{\rho^2+s^2}}. \tag{76}$$

Insertion of Eqs. (74), (75), and (76) into Eq. (73) yields

$$\mathbf{F}_1 = \mathbf{e}_z\frac{Q_T}{16}\left\{\frac{\nu}{s^2} - \frac{\nu s^2}{\left(\rho^2+s^2\right)^2} + \frac{\left[\gamma\left(b^3-a^3\right)-b^3\right]E_p}{s^3} + \frac{\left[\gamma\left(b^3-a^3\right)-b^3\right]E_p s}{\left(\rho^2+s^2\right)^2} - \frac{2\left[\gamma\left(b^3-a^3\right)-b^3\right]E_p s^3}{\left(\rho^2+s^2\right)^3} + \frac{4E_p s}{\sqrt{\rho^2+s^2}} - 4E_p\right\}, \tag{77}$$

where $b\le s\le h-b$. Equation (77) is the force exerted on the charged-particle by the induced charges on the surface of the upper conductor plate.

The expression for the force exerted on the particle by the induced charges on the surface of the lower conductor plate is obtained by inserting $\mathbf{R}_2$ of Eq. (70) into Eq. (68). Repeating the similar procedure outlined in Eqs. (71) and (72), one obtains

$$\mathbf{F}_2 = \mathbf{e}_z\frac{Q_T(h-s)}{4\varepsilon_3}\int_0^{\rho}\frac{\sigma_{ilp}\rho_2 d\rho_2}{\left[\rho_2^2+(h-s)^2\right]^{3/2}}. \tag{78}$$

Insertion of the explicit expression for σ_{ilp} from Eq. (60) into Eq. (78) yields

$$\mathbf{F}_2 = \mathbf{e}_z\frac{Q_T(h-s)}{4}\int_0^{\rho}\left\{\frac{3\left[\gamma\left(b^3-a^3\right)-b^3\right]E_p(h-s)^2}{\left[\rho_2^2+(h-s)^2\right]^4} - \frac{\nu(h-s)+\left[\gamma\left(b^3-a^3\right)-b^3\right]E_p}{\left[\rho_2^2+(h-s)^2\right]^3} - \frac{E_p}{\left[\rho_2^2+(h-s)^2\right]^{3/2}}\right\}\rho_2 d\rho_2. \tag{79}$$

Using the integral formulas from Eqs. (74), (75), and (76) with s replaced by $h-s$, Eq. (79) becomes

$$\mathbf{F}_2 = \mathbf{e}_z\frac{Q_T}{16}\left\{\frac{\nu(h-s)^2}{\left[\rho^2+(h-s)^2\right]^2} - \frac{\nu}{(h-s)^2} + \frac{\left[\gamma\left(b^3-a^3\right)-b^3\right]E_p}{(h-s)^3} + \frac{\left[\gamma\left(b^3-a^3\right)-b^3\right]E_p(h-s)}{\left[\rho^2+(h-s)^2\right]^2} - \frac{\left[\gamma\left(b^3-a^3\right)-b^3\right]E_p(h-s)^3}{\left[\rho^2+(h-s)^2\right]^3} + \frac{4E_p(h-s)}{\sqrt{\rho^2+(h-s)^2}} - 4E_p\right\}, \tag{80}$$

where $b\le s\le h-b$. Equation (80) is the force exerted on the charged-particle by the induced charges on the surface of the lower conductor plate.

For a parallel plate system, which is microscopically large, but macroscopically small, the forces in Eqs. (77) and (80) can be approximated by making ρ go to infinity. This approximation is certainly valid for very small charged-particles confined between large parallel conductor plates. In the limit ρ goes to infinity, Eqs. (77) and (80) simplify in form as

$$\mathbf{F}_1 = \mathbf{e}_z\frac{Q_T}{4}\left\{\frac{\nu}{4s^2} + \frac{\left[\gamma\left(b^3-a^3\right)-b^3\right]E_p}{4s^3} - E_p\right\} \tag{81}$$

and

$$\mathbf{F}_2 = \mathbf{e}_z\frac{Q_T}{4}\left\{\frac{\left[\gamma\left(b^3-a^3\right)-b^3\right]E_p}{4(h-s)^3} - \frac{\nu}{4(h-s)^2} - E_p\right\}, \tag{82}$$

where $b \le s \le h-b$ and v is defined in Eq. (51),

$$v = \frac{2a(b-a)\sigma_1}{\varepsilon_0\kappa_2} + \frac{a^2\sigma_1 + b^2\sigma_2}{\varepsilon_0\kappa_3}.$$

Notice that the resulting forces in Eqs. (81) and (82) are now just one dimensional forces; that is, $\mathbf{F}_1 \equiv \mathbf{F}_1(s)$ and $\mathbf{F}_2 \equiv \mathbf{F}_2(s)$, where the parameter s is the relative distance between the center of mass point of core-shell structured charged-particle and the surface of upper conductor plate. The dynamics of charged-particle system illustrated in Fig. 2 has now reduced down to solving a nonlinear ordinary differential equation.

Insertion of Eqs. (81) and (82) into Eq. (65) yields the total force exerted on the charged-particle by the induced charges on the surfaces of parallel plate conductors. The result is

$$\mathbf{F} = \mathbf{e}_z \frac{Q_T}{16}\left\{\frac{v}{s^2} - \frac{v}{(h-s)^2} + \frac{\left[\gamma\left(b^3-a^3\right)-b^3\right]E_p}{s^3} + \frac{\left[\gamma\left(b^3-a^3\right)-b^3\right]E_p}{(h-s)^3} - 8E_p\right\}.$$

If the gravitational effect is included, the force experienced by the particle is

$$\mathbf{F}_T = \mathbf{F} - \mathbf{e}_z mg$$

or

$$\mathbf{F}_T = \mathbf{e}_z \frac{Q_T}{16}\left\{\frac{v}{s^2} - \frac{v}{(h-s)^2} + \frac{\left[\gamma\left(b^3-a^3\right)-b^3\right]E_p}{s^3} + \frac{\left[\gamma\left(b^3-a^3\right)-b^3\right]E_p}{(h-s)^3} - 8E_p\right\} - \mathbf{e}_z mg, \tag{83}$$

where m is the mass of the particle, $g = 9.8\,\mathrm{m\cdot s^{-2}}$ is the gravity constant, and the gravitational force has been assumed to be in the $-\mathbf{e}_z$ direction. Since Q_T is related to v by

$$Q_T = 4\pi\varepsilon_0\kappa_3 v, \tag{84}$$

the $\mathbf{F}_T$ of Eq. (83) may be re-expressed for convenience as

$$\mathbf{F}_T = \mathbf{e}_z \frac{\pi\varepsilon_0\kappa_3 v}{4}\left\{\frac{v}{s^2} - \frac{v}{(h-s)^2} + \frac{\left[\gamma\left(b^3-a^3\right)-b^3\right]E_p}{s^3} + \frac{\left[\gamma\left(b^3-a^3\right)-b^3\right]E_p}{(h-s)^3} - 8E_p\right\} - \mathbf{e}_z mg. \tag{85}$$

The dynamics of oscillating charged-particle is given by

$$\mathbf{e}_z \frac{d}{dt}\left(\frac{mv}{\sqrt{1-\frac{v^2}{c^2}}}\right) = \mathbf{F}_T, \tag{86}$$

where $c = 3\times10^8\,\mathrm{m\cdot s^{-1}}$ is the speed of light in vacuum. The left hand side of Eq. (86) can be differentiated to give

$$\mathbf{e}_z v \frac{d}{dt}\left(\frac{1}{\sqrt{1-\frac{v^2}{c^2}}}\right) + \frac{\dot{v}\mathbf{e}_z}{\sqrt{1-\frac{v^2}{c^2}}} = \frac{\mathbf{F}_T}{m}, \tag{87}$$

where $\dot{v} \equiv dv/dt$. Knowing that

$$\frac{d}{dt}\left(\frac{1}{\sqrt{1-\frac{v^2}{c^2}}}\right) = \frac{v\dot{v}}{c^2\left(1-\frac{v^2}{c^2}\right)^{3/2}},$$

equation (87) becomes

$$\frac{v^2\dot{v}\mathbf{e}_z}{c^2\left(1-\frac{v^2}{c^2}\right)^{3/2}} + \frac{\dot{v}\mathbf{e}_z}{\sqrt{1-\frac{v^2}{c^2}}} = \frac{\mathbf{F}_T}{m}.$$

Multiplying both sides by $c^2\left(1-v^2/c^2\right)^{3/2}$ yields

$$\dot{v}\mathbf{e}_z = \frac{\mathbf{F}_T}{m}\left(1-\frac{v^2}{c^2}\right)^{3/2}. \tag{88}$$

Since $v = \dot{s}$ and $\dot{v} = \ddot{s}$, Eq. (88) becomes

$$\ddot{s}\mathbf{e}_z = \frac{\mathbf{F}_T}{m}\left(1-\frac{\dot{s}^2}{c^2}\right)^{3/2},$$

where $\ddot{s} \equiv d^2s/dt^2$. With $\mathbf{F}_T$ explicitly inserted from Eq. (85), the expression for $\ddot{s}$ becomes

$$\ddot{s} = \left(1-\frac{\dot{s}^2}{c^2}\right)^{3/2}\left(\frac{\pi\varepsilon_0\kappa_3 v}{4m}\left\{\frac{v}{s^2} - \frac{v}{(h-s)^2} + \frac{\left[\gamma\left(b^3-a^3\right)-b^3\right]E_p}{s^3} + \frac{\left[\gamma\left(b^3-a^3\right)-b^3\right]E_p}{(h-s)^3} - 8E_p\right\} - g\right), \tag{89}$$

where $\mathbf{e}_z$ has been dropped for convenience. It is convenient to re-express Eq. (89) in terms of the variable z_d illustrated in Fig. 2(a). Two variables, s and z_d, are related to each other by

$$s = z_d + b, \quad \dot{s} = \dot{z}_d, \quad \ddot{s} = \ddot{z}_d, \tag{90}$$

where b is a constant. Hence, in terms of z_d, Eq. (89) becomes

$$\ddot{z}_d = \left(1-\frac{\dot{z}_d^2}{c^2}\right)^{3/2}\left(\frac{\pi\varepsilon_0\kappa_3 v}{4m}\left\{\frac{v}{(z_d+b)^2} - \frac{v}{(h-z_d-b)^2} + \frac{\left[\gamma\left(b^3-a^3\right)-b^3\right]E_p}{(z_d+b)^3} + \frac{\left[\gamma\left(b^3-a^3\right)-b^3\right]E_p}{(h-z_d-b)^3} - 8E_p\right\} - g\right). \tag{91}$$

Equation (91) governs the dynamics of an oscillating charged-particle, subjected to high electrostatic fields, at all speeds.

E. Criterion for charged-particle oscillation in the absence of charge transfer process

The criterion for charged-particle oscillation in the absence of charge transfer process between the rebounding electrode

and the charged-particle can be obtained by analyzing the force expression of Eq. (85),

$$\mathbf{F}_T = \mathbf{e}_z \frac{\pi\varepsilon_0\kappa_3 v}{4}\left\{\frac{v}{s^2}-\frac{v}{(h-s)^2} + \frac{\left[\gamma\left(b^3-a^3\right)-b^3\right]E_p}{s^3} + \frac{\left[\gamma\left(b^3-a^3\right)-b^3\right]E_p}{(h-s)^3}-8E_p\right\}-\mathbf{e}_z mg, \qquad (92)$$

The kinematics of charged-particle motion associated with the force $\mathbf{F}_T$ of Eq. (92) is illustrated in Fig. 6, where the parameters s and z_d are related by $s = z_d + b$. For the plot illustrated in Fig. 6, the turning points of charged-particle motion occurs approximately at $z_d = z_{d,m} = 0.25h$.

By definition, when the particle is in vicinity of the turning point, but not past it, the net force acting on the particle is directed in the opposite direction of particle's motion. Immediately past the turning point, the particle's motion is in the same direction as the net force. Thus, immediately past the turning point, the net force satisfies

$$\mathbf{F}_T\left(z_{d,m}\right) > 0$$

or

$$\frac{\pi\varepsilon_0\kappa_3 v}{4}\left\{\frac{v}{z_{d,m}^2}-\frac{v}{\left(h-z_{d,m}\right)^2}+\frac{\left[\gamma\left(b^3-a^3\right)-b^3\right]E_p}{z_{d,m}^3} + \frac{\left[\gamma\left(b^3-a^3\right)-b^3\right]E_p}{\left(h-z_{d,m}\right)^3}-8E_p\right\}-mg>0.$$

Referring to the plot in Fig. 6, this result simply states that net force is in $\mathbf{e}_z$ direction at $z_d = z_{d,m}$. This relation can be rewritten as

$$\overbrace{\left[\frac{\gamma\left(b^3-a^3\right)-b^3}{z_{d,m}^3}+\frac{\gamma\left(b^3-a^3\right)-b^3}{\left(h-z_{d,m}\right)^3}-8\right]}^{\psi}E_p > \frac{v}{\left(h-z_{d,m}\right)^2}-\frac{v}{z_{d,m}^2}+\frac{4mg}{\pi\varepsilon_0\kappa_3 v},$$

where

$$\gamma = \frac{3\kappa_3 b^3}{\left(\kappa_2+2\kappa_3\right)b^3+2\left(\kappa_2-\kappa_3\right)a^3}$$

and

$$\psi = \frac{\gamma\left(b^3-a^3\right)-b^3}{z_{d,m}^3}+\frac{\gamma\left(b^3-a^3\right)-b^3}{\left(h-z_{d,m}\right)^3}-8. \qquad (93)$$

Notice that $0<\gamma<1$; therefore, $\psi<0$. Thus, the previous relation can be rewritten as

$$-\frac{v}{\left(h-z_{d,m}\right)^2}+\frac{v}{z_{d,m}^2}-\frac{4mg}{\pi\varepsilon_0\kappa_3 v} > -\psi E_p = |\psi| E_p.$$

Solving for E_p, I obtain

$$E_p < \frac{1}{|\psi|}\left[\frac{v}{z_{d,m}^2}-\frac{v}{\left(h-z_{d,m}\right)^2}-\frac{4mg}{\pi\varepsilon_0\kappa_3 v}\right].$$

In terms of the effective charge Q_T defined in Eq. (84), this result becomes

$$E_p < \frac{1}{Q_T|\psi|}\left\{\frac{Q_T^2}{4\pi\varepsilon_0\kappa_3}\left[\frac{1}{z_{d,m}^2}-\frac{1}{\left(h-z_{d,m}\right)^2}\right]-16mg\right\}. \qquad (94)$$

By definition, $E_p \geq 0$ because it is the magnitude of electric field. Therefore, the right hand side of Eq. (94) must be positive. But, according to the plot illustrated in Fig. 6, $z_{d,m} < h/2$; and, thus

$$\frac{1}{z_{d,m}^2} > \frac{1}{\left(h-z_{d,m}\right)^2}.$$

For a positive particle, $Q_T > 0$ and Eq. (94) can always be satisfied for a sufficiently ionized positive core-shell structured particle. For convenience, I shall express Q_T in terms of E_p. Equation (94) can be rearranged to yield

$$\frac{Q_T^2}{4\pi\varepsilon_0\kappa_3}\left[\frac{1}{z_{d,m}^2}-\frac{1}{\left(h-z_{d,m}\right)^2}\right]-|Q_T||\psi|E_p-16mg>0.$$

Utilizing the quadratic formula, this can be solved for Q_T to yield

$$Q_T > \frac{2\pi\varepsilon_0\kappa_3}{\xi}\left(|\psi|E_p+\sqrt{\psi^2E_p^2+\frac{16mg\xi}{\pi\varepsilon_0\kappa_3}}\right), \qquad (95)$$

where

$$\xi = \frac{1}{z_{d,m}^2}-\frac{1}{\left(h-z_{d,m}\right)^2} \qquad (96)$$

and

$$\psi = \frac{\gamma\left(b^3-a^3\right)-b^3}{z_{d,m}^3}+\frac{\gamma\left(b^3-a^3\right)-b^3}{\left(h-z_{d,m}\right)^3}-8.$$

When the core-shell structured charged-particle is negatively charged, how does the charged-particle oscillation criterion get modified? For the negatively charged core-shell structured particle, $v<0$, where

$$v = \frac{2a(b-a)\sigma_1}{\varepsilon_0\kappa_2}+\frac{a^2\sigma_1+b^2\sigma_2}{\varepsilon_0\kappa_3}.$$

Thus, the $\mathbf{F}_T$ of Eq. (92) becomes

$$\mathbf{F}_T = \mathbf{e}_z\frac{\pi\varepsilon_0\kappa_3|v|}{4}\left\{\frac{|v|}{s^2}-\frac{|v|}{(h-s)^2} - \frac{\left[\gamma\left(b^3-a^3\right)-b^3\right]E_p}{s^3} - \frac{\left[\gamma\left(b^3-a^3\right)-b^3\right]E_p}{(h-s)^3}+8E_p\right\}-\mathbf{e}_z mg.$$

Furthermore, since $\gamma\left(b^3-a^3\right)-b^3<0$, I have

$$\mathbf{F}_T=\mathbf{e}_z\frac{\pi\varepsilon_0\kappa_3|v|}{4}\left\{\frac{|v|}{s^2}-\frac{|v|}{(h-s)^2}+\frac{\left|\gamma\left(b^3-a^3\right)-b^3\right|E_p}{s^3}+\frac{\left|\gamma\left(b^3-a^3\right)-b^3\right|E_p}{(h-s)^3}+8E_p\right\}-\mathbf{e}_z mg. \tag{97}$$

Now, immediately past the turning point at $z_{d,m}=7.5\times10^{-4}\,\mathrm{m}$ in Fig. 13, the net force acting on the particle satisfies the condition given by

$$\mathbf{F}_T\left(z_{d,m}\right)<0$$

or

$$\frac{\pi\varepsilon_0\kappa_3|v|}{4}\left\{\frac{|v|}{z_{d,m}^2}-\frac{|v|}{\left(h-z_{d,m}\right)^2}+\frac{\left|\gamma\left(b^3-a^3\right)-b^3\right|E_p}{z_{d,m}^3}+\frac{\left|\gamma\left(b^3-a^3\right)-b^3\right|E_p}{\left(h-z_{d,m}\right)^3}+8E_p\right\}-mg<0,$$

where Eq. (97) has been substituted in for the explicit expression. This relation is rearranged as

$$\left[\frac{\left|\gamma\left(b^3-a^3\right)-b^3\right|}{z_{d,m}^3}+\frac{\left|\gamma\left(b^3-a^3\right)-b^3\right|}{\left(h-z_{d,m}\right)^3}+8\right]E_p<\frac{|v|}{\left(h-z_{d,m}\right)^2}-\frac{|v|}{z_{d,m}^2}+\frac{4mg}{\pi\varepsilon_0\kappa_3|v|}.$$

One notices that

$$\frac{\left|\gamma\left(b^3-a^3\right)-b^3\right|}{z_{d,m}^3}+\frac{\left|\gamma\left(b^3-a^3\right)-b^3\right|}{\left(h-z_{d,m}\right)^3}+8=|\psi|,$$

where ψ is defined in Eq. (93). Thus, I have

$$|\psi|E_p<\frac{|v|}{\left(h-z_{d,m}\right)^2}-\frac{|v|}{z_{d,m}^2}+\frac{4mg}{\pi\varepsilon_0\kappa_3|v|}$$

or

$$E_p<\frac{1}{|\psi|}\left[\frac{|v|}{\left(h-z_{d,m}\right)^2}-\frac{|v|}{z_{d,m}^2}+\frac{4mg}{\pi\varepsilon_0\kappa_3|v|}\right].$$

Notice that $|v|$ can be expressed as

$$|v|=\frac{|Q_T|}{4\pi\varepsilon_0\kappa_3},$$

where Eq. (84) has been used. Thus, E_p becomes

$$E_p<\frac{1}{|Q_T\psi|}\left\{\frac{|Q_T|^2}{4\pi\varepsilon_0\kappa_3}\left[\frac{1}{\left(h-z_{d,m}\right)^2}-\frac{1}{z_{d,m}^2}\right]+16mg\right\}. \tag{98}$$

Now, E_p cannot be negative because it is the magnitude of electric field. Since $z_{d,m}>h/2$ in Fig. 13, it must be true that

$$\frac{1}{\left(h-z_{d,m}\right)^2}>\frac{1}{z_{d,m}^2}.$$

Therefore, Eq. (98) can always be satisfied for a core-shell structured particle which is sufficiently charged negatively. Rearranging Eq. (98), I have

$$\frac{|Q_T|^2}{4\pi\varepsilon_0\kappa_3}\left[\frac{1}{\left(h-z_{d,m}\right)^2}-\frac{1}{z_{d,m}^2}\right]-|Q_T\psi|E_p+16mg>0.$$

Introducing η,

$$\eta=\frac{1}{\left(h-z_{d,m}\right)^2}-\frac{1}{z_{d,m}^2},$$

this becomes

$$\frac{|Q_T|^2\eta}{4\pi\varepsilon_0\kappa_3}-|Q_T\psi|E_p+16mg>0.$$

Utilizing the quadratic formula, I find

$$|Q_T|>\frac{2\pi\varepsilon_0\kappa_3}{\eta}\left(|\psi|E_p\pm\sqrt{\psi^2E_p^2-\frac{16mg\eta}{\pi\varepsilon_0\kappa_3}}\right)$$

Since $|Q_T|$ cannot be negative, one must make sure the right side is positive. But, since

$$|\psi|E_p>\sqrt{\psi^2E_p^2-\frac{16mg\eta}{\pi\varepsilon_0\kappa_3}},$$

I have

$$|Q_T|>\frac{2\pi\varepsilon_0\kappa_3}{\eta}\left(|\psi|E_p-\sqrt{\psi^2E_p^2-\frac{16mg\eta}{\pi\varepsilon_0\kappa_3}}\right), \tag{99}$$

where

$$\eta=\frac{1}{\left(h-z_{d,m}\right)^2}-\frac{1}{z_{d,m}^2}.$$

Equation (99) is the oscillation criterion for the negatively charged core-shell structured particle. The resulting form is different from the positively charged case, i.e., Eq. (95), due to the fact that negatively charged particle oscillates near the lower conductor plate whereas the positively charged particle oscillates near the upper conductor plate in Fig. 2.

F. Electromagnetic radiation

It is well known that the oscillating charged-particle radiates electromagnetic energy. With respect to the reference point on the surface of the upper conductor plate, the oscillating charged-particle has a dipole moment given by

$$\mathbf{p}_d=-\mathbf{e}_z Q_T s$$

or

$$\mathbf{p}_d = -\mathbf{e}_z 4\pi\varepsilon_0\kappa_3 \nu s$$

where $\mathbf{p}_d \equiv \mathbf{p}_d(t)$, $s \equiv s(t)$, and Eq. (84) has been inserted for Q_T. The negative sign comes from the fact that the particle is perceived as residing in the negative z-axis to someone on the surface of the upper conductor plate. In terms of $z_d \equiv z_d(t)$ defined in Eq. (90), $\mathbf{p}_d$ becomes

$$\mathbf{p}_d = -\mathbf{e}_z 4\pi\varepsilon_0\kappa_3 \nu (z_d + b),$$
$$\ddot{\mathbf{p}}_d = -\mathbf{e}_z 4\pi\varepsilon_0\kappa_3 \nu \ddot{z}_d,$$

where b is a constant. The electromagnetic power radiated by an oscillating charged-particle, P_{rad}, is given by the Liénard formula,

$$P_{rad} = \frac{1}{6\pi\varepsilon_0 c^3}\left(1 - \frac{\dot{z}_d^2}{c^2}\right)^{-3} \ddot{\mathbf{p}}_d \cdot \ddot{\mathbf{p}}_d$$
$$= \frac{8\pi\varepsilon_0\kappa_3^2\nu^2}{3c^3}\left(1 - \frac{\dot{z}_d^2}{c^2}\right)^{-3} \ddot{z}_d^2.$$

Insertion of Eq. (91) for $\ddot{z}_d$ finally yields

$$P_{rad} = \frac{8\pi\varepsilon_0\kappa_3^2\nu^2}{3c^3}\left(\frac{\pi\varepsilon_0\kappa_3\nu}{4m}\left\{\frac{\nu}{(z_d+b)^2} - \frac{\nu}{(h-z_d-b)^2} + \frac{\left[\gamma\left(b^3-a^3\right)-b^3\right]E_p}{(z_d+b)^3} + \frac{\left[\gamma\left(b^3-a^3\right)-b^3\right]E_p}{(h-z_d-b)^3} - 8E_p\right\} - g\right)^2,$$

where

$$\nu = \frac{2a(b-a)\sigma_1}{\varepsilon_0\kappa_2} + \frac{a^2\sigma_1 + b^2\sigma_2}{\varepsilon_0\kappa_3},$$

which is the result defined in Eq. (17) for the Liénard radiation power.

IV. CONCLUDING REMARKS

The phenomenon of charged-particle oscillation subjected to a constant electric field has been investigated. For a positively charged core-shell structured particle, the criterion for an oscillatory motion is given by

$$Q_T > \frac{2\pi\varepsilon_0\kappa_3}{\xi}\left(|\psi|E_p + \sqrt{\psi^2 E_p^2 + \frac{16mg\xi}{\pi\varepsilon_0\kappa_3}}\right), \qquad (100)$$

where

$$\xi = \frac{1}{z_{d,m}^2} - \frac{1}{\left(h - z_{d,m}\right)^2} > 0,$$

$$\psi = \frac{\gamma\left(b^3-a^3\right)-b^3}{z_{d,m}^3} + \frac{\gamma\left(b^3-a^3\right)-b^3}{\left(h-z_{d,m}\right)^3} - 8 < 0,$$

and

$$\gamma = \frac{3\kappa_3 b^3}{(\kappa_2+2\kappa_3)b^3 + 2(\kappa_2-\kappa_3)a^3} < 1.$$

For the parallel plate configuration illustrated in Fig. 2, the positively charged core-shell structured particle can only have oscillatory modes in region where $0 < z_d < h/2$. This region is further divided into subregions A and B, and this is illustrated in Fig. 8. In this work, the upper conductor plate is located at $z_d = 0$ and the lower conductor plate is located at $z_d = h$. Further, the upper conductor plate is held at voltage V_T and the lower conductor plate has a voltage of V_L, where $V_T > V_L$. That said, the magnitude of a dominant force in region A falls off with distance like $1/s^3$ and this force acts to repulse the positively charged core-shell structured particle from the upper conductor plate. In region B, the magnitude of a dominant force falls of like $1/s^2$ with distance and this force acts to attract the particle towards the upper conductor plate. It is this competition between the two dominant forces from regions A and B that puts particle in an oscillatory motion.

Such oscillatory mechanism does not involve any charge exchange; therefore, it is fundamentally different from the traditional description by charge exchange.[9] Nevertheless, the novel finding in this work does not invalidate the charge exchange description altogether because the two oscillatory phenomena are not exactly the same. For instance, the traditional picture deals with charged particle oscillation in which the particle sweeps the entire gap between the two plates whereas, here, the particle only oscillates in the restricted regions between the plates. Further, here, the charged-particle must be structured and not a "point" particle in order to have any oscillatory motion. The reason for this is because the repulsive force in region A arises as a consequence of induced polarization and a point particle does not have such property. Without such force appearing in region A, there would not be a way to repulse the positively charged particle from sticking to the surface of the upper conductor plate in Fig. 8. The traditional description by process of charge transfer does not have such restrictions, of course. Thus, the two phenomena are not exactly the same. Nonetheless, the novel finding here presents yet another mechanism for a charged-particle oscillation in an otherwise uniform and constant electric field.

For a negatively charged core-shell structured particle, the oscillatory criterion is given by

$$|Q_T| > \frac{2\pi\varepsilon_0\kappa_3}{\eta}\left(|\psi|E_p - \sqrt{\psi^2 E_p^2 - \frac{16mg\eta}{\pi\varepsilon_0\kappa_3}}\right), \qquad (101)$$

where

$$\eta = \frac{1}{\left(h - z_{d,m}\right)^2} - \frac{1}{z_{d,m}^2} > 0.$$

The oscillatory behavior for negatively charged core-shell structured particle is observed only in the region where $h/2 < z_d < h$; and, this is illustrated in Fig. 12. For the case of negatively charged particle, subregions A and B are formed near the lower conductor plate side of Fig. 12, which is exactly

the opposite of the positively charged particle case. Again, the force in region A repulses the particle from the lower conductor plate and the force in region B attracts the particle to the lower conductor plate. It is this "push-pull" competition between the two dominant forces in regions A and B that puts charged-particle in an oscillatory motion. Such oscillatory behavior is only possible because the particle can be polarized under applied electric field.

Because of the explicit mass dependence in Eqs. (100) and (101), the charged particle oscillation discussed in this work is more favorably satisfied by microscopic or smaller particles than by macroscopic counterparts due to various experimental limitations. In principle, particles of any size can be charged to satisfy the oscillation criterion of Eqs. (100) or (101) provided a DC electric field of sufficient strength can be applied without electrical breakdown taking place. Unfortunately, electrical breakdown occurs at some point even in vacuum and this may limit macroscopic particles from satisfying Eqs. (100) or (101).[21]

The charged-particle oscillator based on the presented novel mechanism represents a natural prototype for illuminating electric dipole radiation. In such system, the frequency of emitted electromagnetic radiation is controlled by a DC voltage biased across the two plane-parallel electrodes. The strength of emitted radiation power from such system depends directly on the magnitude of effective charge carried by the charged-particle.

As for potential applications, the finding in this work can be utilized to build a source for generating microwave radiation. Microwaves thus generated, for instance, might be used to heat water or to excite gases in tiny plasma capsules to produce light. As another potential application, the repulsive mechanism discussed here can be utilized to build an antifriction device. Such device would not require any grease or oil, which are known to be environmentally hazardous. Instead, the friction in such device would be controlled by applied DC voltage.

In nanoscale plasma confinements, nanocavities for instance, only scarce number of ionized atoms or particles participate in the dynamics. This is so because only finite number of ionized particles can be contained in such small scale confinement. In such system, effects arising from the collective motion of particles may only be a small perturbation compared to the effects arising from individual particle dynamics. For very large scale systems, wherein enormous number of ionized particles are involved, exactly the opposite is true. There, effects arising from the collective motion of particles become predominant. As the technology evolves, plasma systems will eventually enter the regime of submicron to nanometer scale plasma confinements. Already, the size of display pixels is approaching the dimensions of few visible wavelengths; and, display technologies based on charged particles are beginning to involve fewer ionized nanoparticles, where individual particle effects are no longer small perturbations. In the electronics industry, the finite particle nonneutral plasma systems are becoming technologically very important as nanoscale fabrication processes demand for the development of extreme UV (ultraviolet) to X-ray lasers. For instance, device fabrication process at length scale of $\sim 20\,\mathrm{nm}$ or less by photolithography requires extreme UV lasers. Because solid state devices cannot generate such high frequency laser waves, plasma based sources are the only viable candidates for building extreme UV or X-ray lasers. The macroscopic plasma sources can readily generate extreme UV electromagnetic waves, but at the cost of losing the coherent nature of laser waves. Inevitably, the coherent nature of a laser source demands for finite particle plasma sources, wherein the physics of individual particle dynamics is predominantly important. In this respect, the results obtained in this work should be useful and interesting to certain areas of plasma physics.

V. ACKNOWLEDGMENTS

The author acknowledges the support for this work provided by Samsung Electronics Co., Ltd.

* Electronic address: sungnae.cho@samsung.com

1 R. Tobazeon, J. Phys. D: Appl. Phys. **29**, 2595-2608 (1996).

2 L. Musinski, T. Liu, B. Gilchrist, and A. Gallimore, J. Electrostatics **67**, 54-61 (2009).

3 S. Szirmai, Industry Applications Conference, 2000. Conference Record of the 2000 IEEE (Rome, Italy) **2**, 851 (2000).

4 Th. Trottenberg, H. Kersten, and H. Neumann, New J. Phys. **10**, 063012 (2008).

5 L. Musinski, T. Liu, B. Gilchrist, A. Gallimore, and M. Keidar, Experimental results and modeling advances in the study of nanoparticle field extraction thruster, in: AIAA-2007-5254, 43rd AIAA/ASME/SAE/ASEE Joint Propulsion Conference, Cincinnati, OH, July 8–11, (2007).

6 L. Musinski, T. Liu, B. Gilchrist, A. Gallimore, and M. Keidar, Nanoparticle field extraction thruster (nanoFET): design and results of the microparticle emitter prototype, in: International Electric Propulsion Conference, Florence, Italy, September 17–20, (2007).

7 T. Liu, L. Musinski, P. Patel, A. Gallimore, B. Gilchrist, and M. Keidar, Nanoparticle electric propulsion for space exploration, in: Space Technology and Applications International Forum, Albuquerque, NM, February 11–15, (2007).

8 I. Eu, L. Musinski, T. Liu, A. Deng Di, D. Morris, J. Millunchick, B. Gilchrist, and G. Gallimore, Inkless deposition of microparticles by electrostatic acceleration for materials processing, in: AVS 55th International Symposium and Exhibition, Boston MA, October 19–24, (2008).

9 V. Tulagin, J. Opt. Soc. Am. **59** (3), 328-331 (1969).

10 K. Tamura, Y. Kimura, H. Suzuki, O. Kido, T. Sato, T. Tanigaki, M. Kurumada, Y. Saito, and C. Kaito, Jpn. J. Appl. Phys. **42**, 7489-7492 (2003).

11 R. Sohal, G. Lupina, O. Seifarth, P. Zaumseil, and C. Walczyk, Surface Science **604**, 276-282 (2010).

12 A. Modinos and A. Theophilou, J. Phys. C: Solid State Phys. **4**,

338-353 (1971).
[13] O. Raichev, Phys. Rev. B **73**, 195328 (2006).
[14] N. Jonge, M. Allioux, J. Oostveen, K. Teo, and W. Milne, Appl. Phys. Lett. **87**, 133118 (2005); doi: 10.1063/1.2058225.
[15] C. Edgcombe and N. Jonge, J. Phys. D: Appl. Phys. **40**, 4123 (2007).
[16] Y. Li and H. Cheng, Micro & Nano Lett. **4**(2), pp. 69-73 (2009).
[17] G. Eda, H. Unalan, N. Rupesinghe, G. Amaratunga, Appl. Phys. Lett. **93**, 233502 (2008).
[18] V. Konopsky, S. Sekatskii, and V. Letokhov, J. Phys. IV France **6**, C5-125-C5-128 (1996); doi: 10.1051/jp4:1996520.
[19] H. Iwasaki and K. Sudoh, Jpn. J. Appl. Phys. **41**, 7496-7500 (2002).
[20] O. Kurnosikov, J. de Jong, H. Swagten, and W. de Jonge, Appl. Phys. Lett. **80**, 1076 (2002); doi: 10.1063/1.1448160.
[21] N. Zouache and A. Lefort, IEEE Trans. Dielectr. Electr. Insul. **4** (4), 358-364 (1997); doi: 10.1109/94.625348.